Cold Regions Science and Technology 254 (2027) 105203

Contents lists available at ScienceDirect

Cold Regions Science and Technology

journal homepage: www.elsevier.com/locate/coldregions

Species-specific shrub strategies shape carbon balance and soil processes in high-arctic tundra☆

Carlotta Volterrani [a,c,*], Angela Augusti [a,1], Enrico Brugnoli [a], Federica D'Alò [a], Stefano Moscatello [a], Emanuele Pallozzi [b,d], Olga Gavrichkova [a,d]

[a] Research Institute on Terrestrial Ecosystems (IRET), National Research Council of Italy (CNR), 05010 Porano, Italy
[b] Research Institute on Terrestrial Ecosystems (IRET), National Research Council of Italy (CNR), 00015 Monterotondo, Italy
[c] Department of Environmental Sciences, Informatics and Statistics (DAIS), Cà Foscari University of Venice, 30172 Mestre, VE, Italy
[d] National Biodiversity Future Center (NBFC), 90133 Palermo, Italy

ARTICLE INFO

Keywords:
high-arctic tundra
stable isotope
carbon fluxes
soil microbial activity
shrubification
Dryas octopetala
Salix polaris

ABSTRACT

The expansion of shrub communities in the High Arctic significantly alters carbon (C) and nutrient cycling, yet distinct species are often treated as functionally equivalent in ecosystem models. In this study, we investigated the physiological strategies, plot-scale CO_2 fluxes, and plant-soil-microbe interactions in two dominant high-arctic dwarf shrubs (*Salix polaris* and *Dryas octopetala*) with bare soil included as a reference. Based on multi-year peak-season flux measurement, isotopic characterization ($\delta^{13}C$, $\delta^{15}N$), optical indices, and an *in situ* litter decomposition experiment, we demonstrate that these species differ markedly in their ecological functioning. Dryas consistently outperformed Salix in NEP, GPP, and - under full-sun conditions - R_{eco}, with the magnitude of this difference stable across years. Under full-sun conditions, higher soil water content was associated with lower GPP and NEP in both species, while under cloud conditions this association persisted only in Dryas. Soil temperature and soil water content together explained 50% of the area-normalized GPP variance in Dryas and 28% in Salix under high-light conditions. Isotopic and elemental signatures further reveal different ecological strategies: Salix combined a nitrogen-rich, acquisitive nutrient economy with tight stomatal control and higher intrinsic water-use efficiency, while Dryas had higher C:N ratio and more plastic stomatal regulation, sustaining assimilation under cloudy, low-light conditions. Soil organic C was significantly higher under Dryas (4.2%) than in bare soil (1.5%), with Salix (3.0%) intermediate and not statistically different from either. Total nitrogen (hereafter N) was significantly higher under both shrubs (Dryas 0.22%, Salix 0.25%) relative to bare soil (0.11%), with no significant difference between the two species. Vegetated microsites supported more efficient decomposition of recalcitrant litter than bare soil. Recalcitrant shrub litter retained N during decomposition, while labile litter released it, with potential consequences for N availability under shrub expansion.

Our findings demonstrate that high-arctic shrubs differ in functional traits and physiological strategies, supporting their explicit representation in models of C-nutrient-climate feedbacks.

1. Introduction

Arctic ecosystems are undergoing a period of significant change, driven by greenhouse gas-induced warming and amplified by sea-ice and snow-cover feedbacks - a phenomenon known as Arctic amplification (Serreze and Francis, 2006; Previdi et al., 2020). Arctic environments consequently face interlinked perturbations, including permafrost thaw (Romanovsky and Osterkamp, 2000), shifting in hydrological regimes, and more frequent extreme events such as rain-on-snow occurrences, altering ecosystem productivity and carbon (C) and nutrient cycling, generating feedbacks to the climate system that remain uncertain (McGuire et al., 2012; Jeong et al., 2018; Tarnocai et al., 2009). The warming in the Arctic has not been spatially uniform and the major amplification is registered in waters surrounding Svalbard, placing it

☆ This article is part of a Special issue entitled: '30-y at Dirigibile Italia_CRST' published in Cold Regions Science and Technology.

* Corresponding author at: Research Institute on Terrestrial Ecosystems (IRET), National Research Council of Italy (CNR), 05010 Porano, Italy.
E-mail addresses: carlottavolterrani@cnr.it (C. Volterrani), angela.augusti@cnr.it (A. Augusti), enrico.brugnoli@cnr.it (E. Brugnoli), federicadalo@cnr.it (F. D'Alò), stefano.moscatello@cnr.it (S. Moscatello), emanuele.pallozzi@cnr.it (E. Pallozzi), olga.gavrichkova@cnr.it (O. Gavrichkova).

[1] Deceased: 23 September 2024.

https://doi.org/10.1016/j.coldregions.2026.105203
Received 23 June 2026; Received in revised form 16 October 2026; Accepted 2 November 2026
Available online 5 November 2026
0165-232X/© 2026 The Author(s). Published by Elsevier B.V. This is an open access article under the CC BY license (http://creativecommons.org/licenses/by/4.0/).

among the region's most strongly affected by climate change and making it a natural laboratory for studying high-arctic ecosystem responses (Rantanen et al., 2022; Isaksen et al., 2022).

Warming is a primary driver of the increase in tundra vegetation productivity known as "Arctic greening" (Reichle et al., 2018; Chae et al., 2015; Wenzl et al., 2024) and associated mainly with the expansion of woody shrubs that are reshaping tundra structure and functioning. Concurrently, glacier retreat and active-layer changes expose and modify soils, accelerating decomposition and inducing colonization by microorganisms and vegetation, with consequences for C and nutrient cycling. The ecosystem consequences of greening cannot be inferred from shrub cover alone, because tundra shrub species differ in leaf habit, nutrient economy, water-use regulation, litter quality, and sensitivity to environmental conditions (Myers-Smith et al., 2011).

Understanding how changes in vegetation and soil in the Arctic drive net C uptake or release requires valid proxies of vegetation and microbial functioning. C flux measurements provide insights into whether the ecosystem acts as a C sink or source at a given time and under varying environmental conditions (Chapin et al., 2011; Lafleur et al., 2020). Further partitioning of net ecosystem productivity (NEP) into its component fluxes (e.g. gross primary productivity (GPP) and ecosystem respiration (R_{eco})) enables to assess the sensitivity of different ecosystem compartments to environmental change (Gavrichkova et al., 2020)R_{eco} is a complex flux and includes both plant components, associated with vegetation metabolic demands, and microbial components linked to the decomposition of soil organic matter (SOM) and plant debris (Kuzyakov, 2006). While temperature remains its primary driver, the rate and the range of its variation are further shaped by plant biomass, species, depth of the active layer and substrate availability (Cannone et al., 2016; Wilkman et al., 2018; Kuzyakov and Gavrichkova, 2010).

In Svalbard, due to its geographic isolation, greening is primarily expressed as increased productivity of existing tundra vegetation, with an important contribution from local dwarf shrub (Karlsen et al., 2024; Van der Wal and Stien, 2014). Previous studies reported increased growth and expansion of these communities under rising temperatures (Elmendorf et al., 2012), marked differences in their sensitivity to environmental constraints were also highlighted (Cannone et al., 2016; Van der Wal and Stien, 2014). Much of this evidence stems from single-species experimental manipulations - most notably decades of work on the physiological and phenological responses of *Dryas octopetala* to simulated warming (Welker et al., 1997) - or from single-season field campaigns comparing co-occurring species (Magnani et al., 2022), while multi-year, plot-scale comparisons of C fluxes between co-occurring shrub species under natural field conditions remain scarce. This gap has important consequences: land-surface models still represent Arctic shrubs with a small number of coarse plant functional types, implicitly assuming functional equivalence among co-occurring species (Sulman et al., 2021), and projected Arctic C trajectories are highly sensitive to how shrub productivity and expansion dynamics are represented. (Yazbeck et al., 2025). In this context, our study focused on two shrub vegetation communities: one dominated by *Dryas octopetala* L. and another by *Salix polaris* Wahlenb. The primary objective of this study was to assess how the C balance and its main components respond to environmental drivers in two dominant high-arctic shrub communities, and to determine how species-specific physiological and nutrient-use strategies modulate these responses and influence soil microbial functioning. To achieve these objectives, we carried out a multi-year field study using an integrated approach. Plot-scale CO_2 fluxes were measured in *Dryas*-dominated, *Salix*-dominated and bare soil patches during the peak of the growing season from 2021 to 2024, providing temporally discrete snapshots of ecosystem functioning. To capture more time-integrated ecosystem responses, we employed the use of stable isotopes of C ($\delta^{13}C$) and N ($\delta^{15}N$), and quantified intrinsic water-use efficiency (iWUE), a key trait determining adaptation and productivity strategies (Cowan, 1986; Dudley, 1996). To complete vegetation characterization, leaves reflectance measurements were performed to provide additional information on the physiological status and photosynthetic potential of the target species, allowing the evaluation of interspecific differences in vegetation vigor and pigment concentration. Given the methodological difficulty of measuring microbial activity under field conditions, microbial functional responses to different shrub communities' colonization were assessed using litter decomposition experiments (Parker et al., 2018).

2. Materials and methods

2.1. Study area

The study area was in the Brøgger Peninsula, near Ny-Ålesund (78°57'00.0"N 11°34'00.0"E), a village on the southern coast of Kongsfjorden, in the western side of Spitsbergen Island, Svalbard (Norway). Measurements and sampling were conducted each July from 2021 to 2024, coinciding with the peak of the growing season in this region, as reported by Karlsen et al. (2014). The climate zone is classified as polar tundra (Kottek et al., 2006). According to the Norwegian Centre for Climate Services (Ny-Ålesund station, 78°55'18.5"N 11°55'57.0"E, https://seklima.met.no/observations/), the mean July air temperature for the period 2000-2024 was 6.25 °C. Temperature of this month has increased by 0.0775°C per year, resulting in an increase of 1.86°C for a 21-years period (2000-2024); this trend confirms the observations from previous studies on Svalbard warming (Karlsen et al., 2022; Karlsen et al., 2024). The mean of precipitation was 31.6 mm during the month of July in 2000-2024 period. Snow-melting season ends between late May and late June (Salzano et al., 2023) and snow accumulation starts in late August (Cannone et al., 2016).

The area is underlain by Quaternary carbonate formations, primarily composed of marine littoral deposits and colluvial or weathered materials, with minor contributions from alluvial sediments and peat accumulations. The permafrost is classified as continuous, with a thickness ranging from 75 to 450 meters, and an active layer depth between 0.3 and 1.8 meters (Cannone et al., 2016). The site is a polar semi-desert (Pushkareva et al., 2016), dominated by *Dryas octopetala* L. and *Salix polaris* Wahlenb. Plots were located near Climate Change Tower (CCT), set 1.2 km west of Ny-Ålesund village. Experimental design involved three different communities: *D. octopetala* (hereafter as Dryas), *S. polaris* (hereafter as Salix) and naturally-occurring bare soil (free of aboveground vegetation and roots). For each community, 6 replicate plots (ca. 1 m^2) were established.

2.2. Field measurements of CO_2 fluxes and flux calculation

Flux measurements were performed with different infrared gas analyzers across years: LI-6400XT (LI-COR Environmental, USA) and EGM-5 (PP-System, USA). The analyzers were calibrated against the same certified gas cylinders provided by SIAD (Società Italiana Acetilene e Derivati S.p.A., Italy) before each field campaign. One cylinder was used for zero calibration and consisted of air ($O_2 = 20.95\%$, balance nitrogen) without CO_2. The span cylinder provided contained 402.1 ppmv, with the same O_2 and N_2 proportions as above. All analyzers were equipped with a transparent chamber (14 cm in diameter). For the LI-6400XT, the C flux was calculated by the embedded software at every acquisition over a total of 200 seconds with a rate or 0.1Hz, and the last value was checked for consistency before being retained. EGM-5 fluxes were fitted and calculated with both linear and quadratic curves by the embedded software at the rate of 1Hz, final R^2 values were recorded and the best fit was accepted. Curves with poor fits were discarded. Each plot contained one measurement location for CO_2 fluxes, used repeatedly in four years. CO_2 fluxes were measured under ambient light for NEP and in complete darkness to assess R_{eco}. Ambient light was assessed each time with a MQ-610 PAR meter (400-750 nm, Apogee Instruments, Inc., USA). Measurements were performed at least two times on each plot during the two-week July field campaign each year. In bare soil plots, only

measurements in the dark (R_b) were conducted. Plant-derived respiration (R_{plant}), which encompasses both aboveground (leaves and stems) and belowground (roots and rhizosphere) compounds, was calculated as $R_{plant} = R_{eco}$ - R_b (Kuzyakov, 2006). For this purpose, R_b were averaged to obtain a representative mean value for each measurement day and then subtracted from singular R_{eco} rates. To estimate soil respiration (R_s), which involve microbes, roots and rhizosphere activities of *Dryas* and *Salix* plots without aboveground part were established. R_s measurements were performed at least once per year.

In this study positive values of NEP represent CO_2 uptake (CO_2 sink) by the ecosystem, whereas negative values indicate CO_2 release to the atmosphere (CO_2 source). R_{eco} is considered positive, meaning that higher R_{eco} values correspond to greater CO_2 emissions. GPP, which represents total photosynthetic C uptake, was then calculated as the sum of NEP and R_{eco} ($GPP = NEP + R_{eco}$) (Sakowska et al., 2018). To account for differences in canopy development and plant cover between species and across years, GPP was further normalized by the green area of the vegetation (GPP_n) and expressed as μmol CO_2 m^{-2} s^{-1} per m^2 of green area:

$$GPP_n = \frac{GPP}{Green\ area}$$

Vegetated surface at each flux measurement point was captured with a high-resolution Nikon D610 (Japan) digital camera equipped with a 35mm lens, top-down photograph of each measurement point, at a fixed distance of 50 cm, under consistent lighting conditions to minimize variability. Only the vegetated surface within the flux collar was included in the analysis. Images were analyzed with ImageJ software (Schneider et al., 2012), using the Threshold Color tool (Default thresholding method, HSB color space, dark background), with fixed Hue (47-72), Saturation (122-255), and Brightness (33-246) ranges applied in batch to all images to ensure consistency across the dataset.

To confront the datasets between plant communities and years, we applied a light threshold based on incident photosynthetically active radiation (PAR). Specifically, flux data were separated into two classes, cloud (with PAR < 800 μmol m^{-2} s^{-1}) and full-sun (with PAR ≥ 800 μmol m^{-2} s^{-1}). The threshold of 800 μmol m^{-2} s^{-1} was chosen empirically, after the inspection of scatterplots of fluxes against environmental drivers a clear separation of point clusters below and above this value.

PAR was measured directly during the 2023 and 2024 field campaigns using the quantum sensor integrated into the EGM system. For previous years, PAR data were obtained from an external dataset collected at the study site (Maturilli, 2020). Soil parameters related to C fluxes such as temperature and soil water content (SWC) were measured with a WET sensor (Delta-T Devices Ltd, Cambridge, UK).

2.3. Reflectance measurements

Reflectance measurements at leaf scale were conducted using a PolyPen RP410 UVIS (spectral response range: 380-790 nm; PSI, Drásov, Czech Republic) to assess reflectance in the visible range within the CCT area. GPS coordinates were recorded for each measurement location. The aperture diameter for the leaf measurements was 7 mm, and for each measurement, 10 scans are averaged. The SpectraPen 1.1.0.21 software was used to calculate several spectral indices, including the Normalized Difference Vegetation Index (NDVI: Rouse et al. (1974)), the Greenness Index (G: Zarco-Tejada et al. (2005)), the Modified Chlorophyll Absorption in Reflectance Index (MCARI: Daughtry et al. (2000)) and the Photochemical Reflectance Index (PRI: (Gamon et al., 1997)).

2.4. Vegetation and soil sampling and sample preparation

Leaves of both species were collected in each plot every year from 2021 to 2024 outside the area used for flux measurements. Fresh leaves were collected into paper bag and dried immediately in an oven at 50°C for 48 h. Then, samples were ground into a homogeneous powder using a 4-ball mill (MM 400, Retsch). Soil samples were collected during 2021 and 2022 sampling campaign. Samples were taken with a core drill to a depth of 10 cm. One core per plot was collected, for a total of 18 cores per season campaign (36 cores in total). Each core was taken from a different plot. In Dryas and Salix plots, soil cores were sampled beneath the plant cushions to include the rhizosphere of each species; instead, on bare soil plots, soil cores were taken from the center of the plot. The soil was carefully cleaned of roots and any plant material, then oven-dried at 70°C for 72 h. Afterwards, soil samples were ground in the same way as the as vegetal material.

2.5. Laboratory analyses / C and N analyses

An aliquot of leaves and soil powder was weighed and analyzed for C and N concentration (dry mass basis, %) and isotope composition ($\delta^{13}C$, $\delta^{15}N$). Analyses were performed with an elemental analyzer (model NA 1500, Carlo Erba, Milan, I), coupled with a continuous flow isotope ratio mass spectrometer (ISOPRIME, GV Instruments, Manchester, UK). Plant samples were analyzed directly, whereas soil samples were treated with 10% hydrochloric acid to remove the (Midwood and Boutton, 1998). N elemental composition and $\delta^{15}N$ were determined on non-treated soil samples.

The isotope ratios of C ($R = {}^{13}C/{}^{12}C$) and N ($R = {}^{15}N/{}^{14}N$) were measured to calculate $\delta^{13}C$ and $\delta^{15}N$ (‰) referring to the Vienna-Pee Dee Belemnite (VPDB) and atmospheric N_2 standards, respectively, as:

$$\delta^{13}C \text{ or } \delta^{15}N = \left(\frac{R_{sample}}{R_{std}} - 1\right) x\ 1000$$

where R_{sample} is the isotope ratio of the sample and R_{std} is the isotope ratio of the international standard.

For $\delta^{13}C$ calibration, IAEA-CH-7 Polyethylene Foil ($\delta^{13}C = -32.15‰$), IAEA-CH6 sucrose ($\delta^{13}C = -10.43‰$), and IAEA-600 caffeine ($\delta^{13}C$ = -27.5‰) were used to scale the measurements to the Vienna Pee Dee Belemnite (VPDB) international standard. For $\delta^{15}N$ calibration, IAEA-600 caffeine ($\delta^{15}N = +1‰$), USGS40 L-Glutamic Acid ($\delta^{15}N = -4.5‰$), and IAEA-NO-3 potassium nitrate ($\delta^{15}N = +4.7‰$) were used to normalize results to the atmospheric N_2 standard (Portarena et al., 2024). For both $\delta^{13}C$ and $\delta^{15}N$, the standard deviation of replicate measurements for each standard and sample was 0.1‰.

2.6. Calculation of c_i /c_a and iWUE

To evaluate stomatal control and C absorption efficiency, the ratio of intercellular to ambient CO_2 concentrations (c_i /c_a) was analyzed. This measure provides a physiological understanding of the variations in $\delta^{13}C$ among species and environmental situations. It is inversely related to $\delta^{13}C$ and represents the balance between CO_2 diffusion into the leaf and its fixation by photosynthesis (Farquhar et al., 1982). Leaf C isotope discrimination (Δ, ‰) of Dryas and Salix was determined as:

$$\Delta = \frac{(\delta_a - \delta_p)}{(1 + \delta_p)} \quad (1)$$

where δ_p is the $\delta^{13}C$ of leaves dry matter and δ_a represent the $\delta^{13}C$ of tropospheric CO_2. Values for δ_a were -8.80‰ in 2021, -8.83‰ in 2022, -8.85‰ in 2023 and -8.84‰ in 2024. Data were provided by the NOAA Network, thanks to the University of Colorado, Institute of Arctic and Alpine Research Stable Isotope Laboratory (INSTAAR-SIL) [http://gml.noaa.gov/outreach/isotopes/].

The Δ values were then used to determine c_i /c_a using the model of Farquhar et al. (1982) as:

$$\frac{c_i}{c_a} = \frac{(\Delta - a)}{(b - a)} \quad (2)$$

where a is the isotopic fractionation during diffusion of CO_2 in air (4.4‰) and b is the isotopic fractionation associated with the enzymatic (Rubisco) carboxylation (27‰).

iWUE [μmol CO_2 mol^{-1} H_2O] is determined by the atmospheric CO_2 concentration and the ratio of atmospheric CO_2 to intracellular CO_2 (2)

$$iWUE = \frac{A}{g_s} = \frac{c_a\left(1-c_i/c_a\right)}{1.6} \quad (3)$$

where A is the rates of C assimilation, g_s is the stomata conductance and the factor 1.6 is the ratio of the diffusivities of water vapor and CO_2 in air (Farquhar and Richards, 1984).

2.7. Environmental data and seasonal integration

To relate leaf isotopic composition and elemental concentrations to environmental conditions experienced during the growing season, atmospheric and soil variables were integrated over a biologically relevant time window. Air temperature and precipitation were obtained from publicly available atmospheric datasets (Boike et al., 2022), while volumetric water content (VWC) and soil temperature at 11 cm depth were retrieved from soil monitoring datasets available for the study site (Grünberg et al., 2025). The start of the growing season was estimated for each year using Sentinel-2 Level-2A satellite imagery (Copernicus Sentinel-2 (processed by ESA), 2022), based on visual assessment of snow cover disappearance in the study area. This indicator was accepted as a proxy of the onset of the growing season. Due to interannual variability in snowmelt timing, this procedure was applied independently for each of the four study years. For each year, environmental variables were extracted from the estimated start of the growing season until the date of leaf sampling. Data were temporally integrated by calculating mean values over this period, thereby providing seasonally averaged environmental conditions. These integrated variables were subsequently used to assess relationships with leaf bulk isotopic signatures and elemental concentrations.

2.8. Litter decomposition

The impact of plant community on microbial activity was assessed through a litter decomposition experiment. Two local species with contrasting litter quality were selected: a labile /high-quality litter type (hereafter LL) was represented by standing leaves of *Carex rupestris*, characterized by high cellulose and hemicellulose content and a recalcitrant litter type (hereafter RL) obtained from freeze-damaged parts of Dryas, rich in lignin. Salix litter was not considered in this experiment because it produces low amount of homogeneous standing litter suitable for standardized decomposition assays (data not shown), whereas Carex litter is abundant, chemically of a good quality (lignin <20%), and is widely distributed at the study site.

Collected litter was oven-dried at 50 °C for 72 h, cleaned of soil particles and coarse debris, cut into small pieces (< 1 cm) and homogenized. Then an amount of ~300 mg was weighed into pre-weighed nylon bags (20 μm mesh). In each Dryas, Salix and bare soil plot, three LL- and three RL-containing bags were buried at 7 cm depth in July 2021. Paired LL and RL bags were retrieved after 1 month, 1 year, and 2 years. Upon retrieval, bags were cleaned from soil particles, oven-dried at 50 °C to constant weight and weighted. Then, the litter was homogenized to a fine powder for C and N elemental and stable isotope composition analyses which was performed similarly to plant material as already described. Percentage of initial mass remaining was calculated as:

$$Mass\ rem = \frac{Mass_{tx}}{Mass_{t0}} * 100$$

Where $Mass_{tx}$ is litter mass at time x and $Mass_{t0}$ is initial mass.

Remaining C (C_{rem}) and remaining N (N_{rem}) were calculated as the following:

$$C_{rem} = \left(\frac{Mass_{tx} * C_{tx}}{Mass_{t0} * C_{t0}}\right) * 100 \; N_{rem} = \left(\frac{Mass_{tx} * N_{tx}}{Mass_{t0} * N_{t0}}\right) * 100$$

Where C_{tx} and N_{tx} are C and N concentrations in time x and C_{t0} and N_{t0} - initial C and N concentrations.

The isotope composition of the lost C and N was calculated with mass balance approach only for LL because changes in mass in RL were too small for reliable model application:

$$\delta lost(C, N) = \frac{\delta_{t0} * Mass_{t0} - \delta_{tx} * Mass_{tx}}{Mass_{t0} - Mass_{tx}}$$

where δ_0 and δ_x is isotope composition of C and N at time x and time 0; $Mass_{t0}$ and $Mass_{tx}$ is litter mass at time x and time 0.

Obtained dataset was used to calculate the decomposition constant (k): remaining mass was log-transformed and regressed against time where k corresponds to the negative slope of the linear regression. The regression was performed using the LINEST function in Microsoft Excel, which returns the slope and intercept of the linearized decay model; k was extracted as k = -slope. Slopes with positive values were excluded from the analyses. Turnover time was calculated as 1/k.

2.9. Chemical characterization of the litter

The determination of cell wall components was carried out following the National Renewable Energy Laboratory (NREL) protocols (TP-510-42618 and TP-510-42619), with minor modifications as described by Santi et al. (2015). Briefly, after the removal of water- and ethanol-soluble extractives and their gravimetric quantification, the extractive-free solid residue was subjected to a two-step acid hydrolysis for the determination of structural carbohydrates and lignin. After hydrolysis, the slurry was vacuum-filtered through a calibrated glass fiber filter to separate the solid and liquid fractions. The acid-insoluble lignin (Klason lignin) was determined gravimetrically from the solid residue retained on the filter. Monomeric sugars released during acid hydrolysis (glucose, arabinose, galactose, and xylose) were quantified in the hydrolyzed liquor by high-performance anion-exchange chromatography with pulsed amperometric detection (HPAEC-PAD) using a Dionex™ ICS-5000 system (Thermo Fisher Scientific, Waltham, MA, USA) equipped with a gold working electrode (1 mm diameter) and an Ag/AgCl reference electrode as described by Santi et al. (2015). Cellulose content was calculated from the glucose released during acid hydrolysis, applying an anhydro correction factor of 0.9 to account for glycosidic bond cleavage, and correcting for starch-derived glucose where applicable. Hemicellulose content was determined as the sum of arabinose, galactose, and xylose concentrations.

2.10. Measurement of soluble sugars and starch

The determination of litter non-structural carbohydrates was carried out following Moscatello et al. (2017), with minor modifications. Briefly, dry and finely ground litter (≈10-20 mg) was extracted with hot water. Samples were incubated at 80 °C for 45 min with gentle agitation, cooled, and centrifuged at 14,000 g for 5 min. Supernatants containing soluble sugars were collected and stored at -20 °C. Pellets for starch analysis were washed four times with 40 mM acetate buffer (pH 4.5) and centrifuged (16,000 g, 5 min). The final pellet was autoclaved (120 °C, 45 min) in acetate buffer to solubilize starch. After cooling, α-amylase (4 U) and amyloglucosidase (40 U) were added, and samples were incubated at 50 °C for 1 h to convert starch to glucose.

Soluble sugars (glucose, fructose, sucrose) and glucose from starch hydrolysis were quantified by enzyme-coupled spectrophotometric assays (Scartazza et al., 2017).

2.11. Data analysis

Analyses were performed using STATISTICA 10 (StatSoft Inc.) and R v4.4.1 (R Core Team, 2025), utilizing *tidyverse* (Wickham et al., 2019) *ggplot2* (Wickham, 2016), *lmerTest and lme4* (Bates et al., 2015) and *emmeans* (Lenth and Piaskowski, 2026) packages. Normality and homogeneity of variances were verified via Shapiro-Wilk and Levene's tests. Parametric data were analyzed using two-way ANOVA (Species × Year) followed by Tukey's HSD post hoc test; non-parametric data were assessed via Kruskal-Wallis and Dunn's tests. Statistical significance was set at $p < 0.05$.

Because plot-scale CO_2 fluxes (NEP, GPP, GPP_n, R_{eco}) were measured repeatedly on the same six plots per species across the four study years, these variables were analyzed using Linear Mixed-Effects Models (LMMs) with plot as a random intercept and Species, Year, and their interaction as fixed effects, fitted separately for full-sun (PAR ≥ 800 μmol m^{-2} s^{-1}) and cloud (PAR < 800 μmol m^{-2} s^{-1}) conditions. Omnibus significance of fixed effects was evaluated with Type III F-tests based on estimated marginal means (joint tests function, *emmeans* package), which is robust to the unbalanced sampling design. Where the Species × Year interaction was significant, Dryas-Salix comparisons were carried out separately for each year (*emmeans*, Šidák-adjusted); otherwise, a single comparison pooled across the study period is reported.

Due to the high variability of Arctic weather conditions during the measurements campaigns, full-sun and cloud conditions are not represented in every year (full-sun: 2021, 2023, 2024; cloudy: 2021, 2022, 2024). Sample sizes ranged from 3 to 6 plots per species, year, and light condition. All reported estimates are accompanied by their standard error, and estimated marginal means (rather than raw group means) are used throughout to account for the unbalanced and repeated-measures structure of the dataset. Repeated measurements of litter decomposition (mass, C, N, isotopes) were analyzed using LMMs with plot as a random intercept. Fixed effects included plant community, time, and litter type. Decomposition constants (k) were analyzed via two-way ANOVA. Significance was assessed using Type III F-tests (*lmerTest, car* packages), followed by Šidák post-hoc comparisons (*emmeans* package) at $p < 0.05$. Reflectance indices were analyzed via one-way ANOVA followed by Tukey's HSD post hoc test. Relationships between C fluxes and environmental drivers (PAR, soil temperature and SWC) were first explored using Pearson correlations with pairwise deletion using the *psych* package (Revelle, 2025). The relationship of R_{plant} with soil temperature and SWC was then assessed with a multiple linear regression ($R_{plant} \sim Soil\ Temp + SWC$; OLS, *stats* package), fitted separately for each species and on data pooled across light conditions. For GPP_n, since Pearson correlations and OLS regressions do not account for repeated measurements on the same plots or for covariation among drivers, we used LMMs with plot as a random intercept, fitted separately for each species and light condition: $GPP_n \sim Soil\ Temp + SWC$; $GPP_n \sim PAR + Soil\ Temp + SWC$. Predictors were standardized (z-scores) prior to fitting to obtain standardized coefficients, and model performance was evaluated via marginal and conditional R^2 (*MuMIn* package; Bartoń, 2026).

Multicollinearity was excluded using a Variance Inflation Factor (VIF) threshold of 5 (*car* package) (Fox and Weisberg, 2019; Hair et al., 2019; Zuur et al., 2010). Finally, analyses involving time-integrated traits (isotopes, nutrients) were performed on aggregated datasets without light-level partitioning.

3. Results

3.1. C fluxes on bare soil and vegetation

Across the study period, NEP was consistently higher in Dryas than in Salix under both cloud ($p < 0.001$) and full-sun conditions ($p < 0.0001$) (Fig. 1A, B), with no significant Species × Year interaction under either light regime. Within-species comparisons showed that Dryas NEP increased significantly under full-sun conditions between 2021 and 2024 ($p < 0.0001$), while no significant interannual variation was found for Dryas under cloud conditions or for Salix under either light

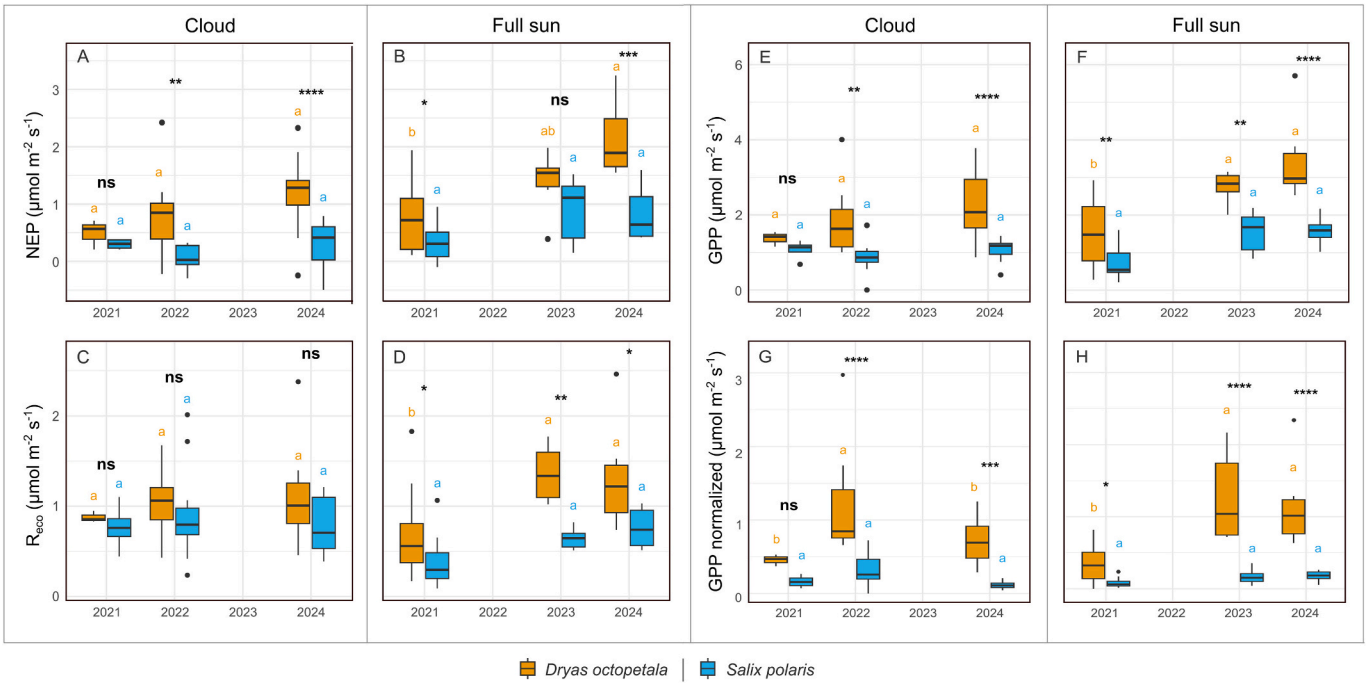


Fig. 1. Boxplots display interannual variability of NEP (A, B), R_{eco} (C, D) and GPP (E, F) and GPP_n (G, H) between Dryas and Salix across years (n=3-6). Species and Year effects were assessed using Linear Mixed-Effects Models with plot as a random intercept, followed by Šidák-adjusted post-hoc comparisons. Statistical differences are expressed as **** $p < 0.0001$, *** $p < 0.001$, **$p < 0.01$, *$p < 0.05$; ns = not significant. Different colored letters indicate significant inter-annual differences within each species, whereas black symbols denote significant differences between the two species within the same year. Because of high weather variability during fieldwork, missing data are present.

condition. R_{eco} (Fig. 1C, D) did not differ significantly between species under cloud conditions, but was significantly higher in Dryas under full-sun conditions ($p < 0.0001$). Dryas R_{eco} was significantly lower in 2021 than in both 2023 and 2024 under full-sun conditions ($p < 0.01$ for both comparisons), with no significant difference between 2023 and 2024. GPP (Fig. 1E, F) was consistently higher in Dryas than in Salix under cloud ($p < 0.001$) and full-sun conditions ($p < 0.0001$), with no significant Species × Year interaction. Dryas GPP increased significantly under full-sun conditions between 2021 and both 2023 and 2024 ($p < 0.01$ for both), remaining stable thereafter; no significant interannual variation was found for Dryas under cloud conditions, nor for Salix under either light condition. GPP_n (Fig. 1G, H) was consistently and markedly higher in Dryas than in Salix. Under cloud conditions, this difference was stable across the study period ($p < 0.0001$), although Dryas GPP_n itself varied significantly among years, increasing from 2021 to 2022 ($p < 0.01$) and subsequently declining from 2022 to 2024 ($p < 0.05$), with 2021 and 2024 values not significantly different from each other. Salix GPP_n showed no significant interannual variation under cloud conditions. Under full-sun conditions, the Species × Year interaction was significant ($p < 0.001$), and Dryas showed significantly higher GPP_n than Salix in every year with available data. Within Dryas, full-sun GPP_n increased sharply from 2021 to both 2023 and 2024 ($p < 0.0001$ for both) and remained stable between 2023 and 2024, while Salix showed no significant interannual variation under full-sun conditions. Overall, Dryas consistently outperformed Salix in NEP, GPP, and - under full-sun conditions - R_{eco}, with the magnitude of this difference stable across years. While the pooled Dryas-Salix contrast was highly significant for NEP, GPP, and GPP_n under cloud conditions, year-specific comparisons did not reach significance in 2021 for these variables, coincident with reduced plot replication that year ($n = 3$ Dryas, $n = 4$ Salix, vs. $n = 6$ in other years); the estimated difference nonetheless remained in the same direction in every year, consistent with reduced statistical power rather than an absent effect.

The analysis of R_{plant} revealed significant inter-specific variability between 2021 and 2024 across years (Fig. S1). Under cloud conditions, R_{plant} of Dryas and Salix remained statistically comparable across the years. In contrast, during full-sun conditions, Dryas exhibited a statistically significant increase in R_{plant}, outperforming Salix in 2023 ($p < 0.01$).

3.2. Reflectance indexes

Reflectance indices (NDVI, MCARI, PRI, and G) exhibited distinct dynamics between 2022 and 2024 (Tab. 1). NDVI was significantly higher in Salix than in Dryas in both 2022 ($p < 0.01$) and 2024 ($p < 0.001$). Temporally, both species experienced a significant reduction in NDVI and G index from 2022 to 2024. However, this decline was much more pronounced in Dryas plots. The MCARI index remained stable across years for Salix ($p > 0.05$), whereas it experienced a sharp and highly significant drop in Dryas from 2022 to 2024 ($p < 0.001$). As a result, while MCARI did not differ significantly between species in 2022, Salix showed significantly higher values than Dryas in 2024 ($p < 0.001$). Conversely, PRI showed no significant temporal variation for either species between 2022 and 2024. Nevertheless, consistent interspecific differences were observed: Salix maintained significantly higher (less negative) PRI values than Dryas in both 2022 ($p < 0.01$) and 2024 ($p < 0.001$).

3.3. Elemental and isotopic composition in soil and leaves samples

Leaf stable isotopes and elemental composition highlighted distinct physiological and nutritional strategies between the two dwarf shrub communities (Fig. 2). Leaf 13C indicated contrasting water-use strategies between species, with Salix leaves being significantly more enriched in ^{13}C than Dryas in 2021 ($p < 0.001$), 2023 ($p < 0.001$), and 2024 ($p < 0.001$) (Fig. 2B). Consequently, during these same years, Salix exhibited significantly lower c_i/c_a ratios ($p < 0.001$ in 2021, 2023 and 2024; Fig. 2C) and a higher iWUE (Fig. 2D) compared to Dryas. These interspecific differences were absent in 2022. Dryas showed a progressive physiological shift across the study period with significantly decline in c_i/c_a and increase in iWUE by 2024. In contrast, Salix maintained a more stable water-use strategy, with the exception of a significant c_i/c_a peak in 2022. Nutrient proxies also diverged between species (Fig. 2B, E). The C:N ratio was significantly higher in Dryas than in Salix in 2021 ($p < 0.001$), 2023 ($p = 0.01$), and 2024 ($p < 0.001$). Analysis of intra-annual dynamics revealed that Dryas maintained a highly stable C:N ratio across all four years. Conversely, Salix experienced a significant shift, with C:N values increasing after the first year of study. Finally, ^{15}N exhibited high interannual variability and weak species-specific separation, with Salix showing significantly higher values than Dryas only in 2021 ($p < 0.01$).

SOC and TN concentrations were generally higher in soils associated with shrub communities than in bare soil (Tab. 2). SOC concentration was significantly higher in soil associated with Dryas (median 4.2%) compared to bare soil (1.5%). However, SOC under Salix (3.0%) showed intermediate values, not differing significantly from either bare soil or Dryas. In contrast, TN concentrations were significantly higher beneath both plant communities (Dryas: 0.22%; Salix: 0.25%) compared to bare soil (0.11%). Significant differences between vegetated and bare soils were also found for $\delta^{13}C$ isotopic composition, with more negative values recorded beneath Dryas (-26.3‰) and Salix (-26.0‰) compared to bare soil (-25.4‰). On the other hand, there were no significant differences in $\delta^{15}N$ among the three groups. Notably, soil under Salix and Dryas did not differ significantly from each other for any of the parameters analyzed.

3.4. The role of environmental factors

The relationships between ecosystem C fluxes (NEP, GPP, GPP_n, R_{eco} and R_{plant}) and main environmental drivers (soil temperature, SWC, and PAR) were evaluated using Pearson correlation matrices under different light conditions (Fig. 3). Under full-sun conditions, C fluxes in both

Table 1
Mean values and standard deviations of spectral indices (NDVI, MCARI, PRI and G) for Dryas and Salix during the 2022 and 2024 growing seasons. The number of observations (N) is reported for each species and year. Statistical analyses were performed using one-way ANOVA followed by Tukey's HSD post-hoc test. Different superscript letters within each column indicate statistically significant differences between species and years ($p < 0.05$). Specifically, lowercase letters (e.g., a, b) denote significant interannual differences within the same species, whereas uppercase letters (e.g., A, B) indicate significant interspecific differences between Dryas and Salix within the same year.

Specie	Year	NDVI (Mean ± SD)	MCARI (Mean ± SD)	PRI (Mean ± SD)	G (Mean ± SD)	N
Dryas	2022	0.715 ± 0.106 **aA**	0.194 ± 0.100 **aA**	-0.019 ± 0.026 **aA**	2.082 ± 0.485 **aA**	51
Dryas	2024	0.602 ± 0.148 **bA**	0.101 ± 0.058 **bA**	-0.024 ± 0.020 **aA**	1.558 ± 0.365 **bA**	20
Salix	2022	0.754 ± 0.046 **aB**	0.171 ± 0.056 **aA**	-0.007 ± 0.025 **aB**	2.183 ± 0.308 **aA**	100
Salix	2024	0.733 ± 0.036 **bB**	0.155 ± 0.050 **aB**	-0.004 ± 0.014 **aB**	1.950 ± 0.265 **bB**	39

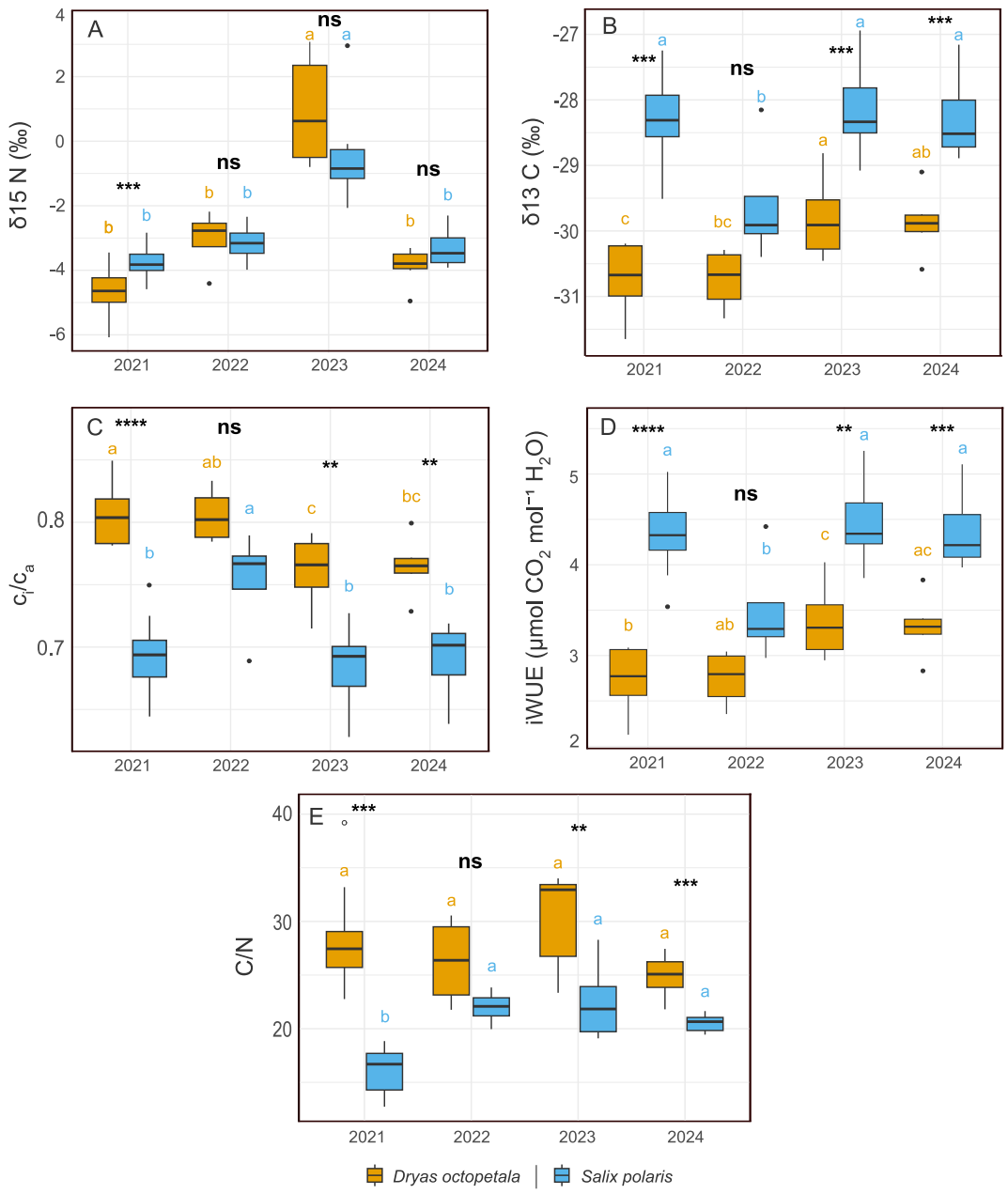


Fig. 2. Boxplots display variability of $\delta^{13}C$ (A), $\delta^{15}N$ (B), c_i/c_a (C), iWUE (D) and C/N ratio (E) between Dryas and Salix. Normal data distribution was verified trough Shapiro-Wilk test. Interspecific differences within each year were evaluated using a two-way ANOVA followed by Tukey's HSD post-hoc test. Statistical differences between species in each year are expressed referred to p-values: * $p \leq 0.05$; ** $p \leq 0.01$; *** $p \leq 0.001$; **** $p \leq 0.0001$; ns = not significant. Intraspecific differences across years were analyzed using the non-parametric Kruskal-Wallis test followed by Dunn's post-hoc test (indicated by lowercase letters; different letters denote significant differences at $p < 0.05$)

Dryas and Salix communities were positively correlated with soil temperature. SWC was negatively correlated with NEP and GPP in both species, whereas the correlation with GPP_n was significant in Dryas only ($p < 0.01$). R_{eco} showed no significant correlation with SWC in either community. R_{plant} was positively correlated with soil temperature in both species (Dryas $p < 0.01$; Salix $p < 0.001$) and negatively correlated with SWC in Dryas ($p < 0.05$), though not significantly in Salix ($p > 0.05$). A regression model, combining both drivers and data from all light conditions, explained a significant portion of R_{plant} variance (Fig. S2) in Dryas ($p = 0.0019$), with soil temperature positively associated with R_{plant} (coeff. = 0.116, $p = 0.037$) and SWC negatively associated with it (coeff. = -0.044, $p = 0.012$). In Salix, by contrast, this combined model did not explain R_{plant} variance, as neither driver was significantly associated with it (SWC: $p = 0.66$; soil temperature: $p = 0.07$).

Furthermore, the correlation matrices highlighted significant temporal dynamics under full-sun conditions. In both Dryas and Salix plots, incident PAR was negatively correlated with soil temperature and positively correlated with SWC. Under high-light conditions, PAR was negatively correlated with GPP, R_{eco}, and R_{plant} for both species but only with Dryas for GPP_n. Mixed-effects models including soil temperature and SWC explained 50% of the variance in GPP_n in Dryas and 28% in Salix under full-sun conditions (marginal R^2). In these models, soil temperature and SWC were both significant in Dryas ($p = 0.007$ and $p = 0.019$, respectively), whereas only soil temperature was significant in Salix ($p = 0.034$). When PAR was added to these models, it was not significant in either species. Soil temperature ($p = 0.004$) and SWC ($p = 0.005$) remained significant predictors in Dryas, whereas none of tested drivers was significant for Salix. Under cloud conditions, correlations

Table 2
Variability of SOC and TN (%), $\delta^{13}C$ in soils under Dryas, Salix and bare soil (n = 12 per type: six cores × two sampling campaigns, 2021 and 2022). Non-normal data distribution was verified through Shapiro-Wilk test. Differences among species were analyzed using the non-parametric Kruskal-Wallis test followed by Dunn's post-hoc test (indicated by lowercase letters; different letters denote significant differences at $p < 0.05$)

Driver	Species	Median [Q1 ~ Q3]	Significance
$\delta^{13}C$	Soil	-25.362 [-25.512 ~ -25.209]	**a**
	Dryas	-26.346 [-26.996 ~ -25.554]	**b**
	Salix	-25.982 [-27.031 ~ -25.875]	**b**
$\delta^{15}N$	Soil	2.851 [0.767 ~ 3.951]	a
	Dryas	1.946 [0.767 ~ 4.409]	a
	Salix	2.281 [1.192 ~ 2.768]	a
SOC	Soil	1.495 [1.17 ~ 2.075]	**a**
	Dryas	4.229 [1.659 ~ 5.788]	**b**
	Salix	3.033 [2.039 ~ 6.205]	**ab**
TN	Soil	0.106 [0.094 ~ 0.121]	**a**
	Dryas	0.218 [0.124 ~ 0.371]	**b**
	Salix	0.25 [0.157 ~ 0.364]	**b**

between C fluxes and environmental drivers weakened considerably, revealing divergent patterns between the two shrub communities. The positive correlation between soil temperature and C fluxes disappeared entirely, with no significant correlations with any flux, including R_{plant} for either species. In Salix plots, C fluxes were no longer significantly correlated with any monitored environmental drivers. In contrast, Dryas NEP and GPP maintained a significant negative correlation to SWC, but not with GPP_n, while R_{eco} and R_{plant} showed no significant correlation with any driver.

Environmental drivers showed moderate reciprocal correlations (Table S1), but multicollinearity was not a concern, as confirmed by Variance Inflation Factors (VIF), all being below 2.5.

3.5. Correlation between stable isotopes, elemental concentration and environmental factors

Figure S3 reports correlations between $\delta^{13}C$ and $\delta^{15}N$ and environmental factors for the Dryas and Salix communities from 2021 to 2024. Overall, the isotopic signatures remained relatively stable across the study period, showing no significant differences between the two shrub species or across the monitored years. In turn, leaf %N exhibited species-specific relationships with seasonally integrated environmental variables (Fig. S4, Panel A- D). In Salix, %N was strongly and negatively correlated with mean air temperature ($R^2 = 0.98$, $p < 0.01$) and mean soil temperature at 11 cm depth ($R^2 = 0.93$, $p < 0.05$), while a positive but marginal relationship was observed with mean volumetric water content (VWC; $R^2 = 0.86$, $p < 0.05$). These results indicate that higher leaf %N in *Salix* was associated with cooler and wetter growing-season conditions. In contrast, *Dryas* showed no significant relationship between leaf %N and temperature-related variables but exhibited a strong positive correlation with cumulative precipitation integrated over the growing season ($R^2 = 0.91$, $p = p < 0.05$).

3.6. Litter chemical composition

Table 3 reports the cell-wall component content of the two litter types, together with the concentrations of non-structural carbohydrates. The two litters were characterized by markedly distinct chemical profiles: in *LL* litter, hemicellulose constituted the dominant fraction, whereas in *RL* lignin was the most abundant component. No differences were detected in ash or extractive content between species; however, lignin, cellulose, and hemicellulose differed significantly. Although the combined proportion of these three components is similar in both litters (≈60%), *RL* contained more than twice as much lignin as *LL*. Conversely, the lower lignin content in *LL* is offset by approximately double the cellulose and hemicellulose content relative to *RL*. These contrasting chemical compositions reflect fundamental anatomical differences: *LL* tissues possess only primary cell walls, where cellulose and hemicellulose constitute the major structural polysaccharides, whereas *RL* forms secondary cell walls typically characterized by high lignin concentrations (Panshin and de Zeeuw, 1980).

The concentration of non-structural carbohydrates also differed significantly between species. Soluble sugars were higher in *LL*, whereas no significant differences were detected in starch content. Overall, non-structural carbohydrate concentrations were considerably lower than values typically reported in the literature (Sauter and Wellenkamp, 1998; Zhou et al., 2022), likely reflecting carbohydrate consumption during tissue senescence. Despite their low concentrations, soluble sugars and starch remain reliable indicators of early litter decomposition because they are among the first substrates to be consumed (Berg, 2000).

3.7. Litter decomposition pattern

Litter type and time significantly affected decomposition (respectively, $p < 0.001$ and $p < 0.001$), with LL decomposing more rapidly, particularly in early phases. Plant community had no significant main effect on decomposition, but a marginal treatment × time interaction ($p = 0.062$), suggesting community influences on decomposition rates. No significant three-way interaction was detected. LL decomposed rapidly within the first month in all plots (Dryas, Salix, Soil), with no significant differences among them (Fig. 4). After one year, mass remaining was again similar across communities. Between first and second year, LL decomposition had largely stabilized in Dryas and Soil plots, whereas Salix plots showed an additional decline in mass. This resulted in a significant difference between Salix and Soil after two years, while Salix and Dryas remained statistically indistinguishable.

RL decomposed slowly than LL (Fig. S6). After one month, no clear variation in litter mass was registered. By one year, Soil plots retained significantly more RL than Dryas plots ($p < 0.01$), while Salix displayed intermediate values and did not differ significantly from either community. After two years, RL mass remaining in Salix and Dryas plots converged, whereas Soil plots continued to show the slowest decomposition.

Decomposition constant (k) differed strongly between litter types ($p < 0.001$) and among plant communities ($p < 0.05$), whereas their interaction was not significant ($p = 0.160$). Within LL, k was higher in Salix than in Soil plots ($p < 0.05$), whereas Dryas and Soil did not differ. Within RL, k didn't significantly differ among communities, likely because of some missing values due to positive slope in individual replicates. Different litter types were characterized by substantial differences in terms of turnover time, which ranged between 7 and 9 years for LL and 17 and 50 years for RL (Tab. S2).

In terms of remaining C and N, the strongest effects were associated with litter type ($p < 0.001$ for both C_{rem} and N_{rem}) and litter type × time interaction ($p < 0.001$ for both). C_{rem} declined more strongly in LL than in RL, consisting with the higher degradability of LL. As for N_{rem}, LL showed a reduction during the first year, followed by stabilization, indicating net N mineralization. RL showed an increase in N_{rem}, indicating N retention in litter over time. Although plant community did not affect C_{rem} and N_{rem} when averaged across all sampling times, the significant community × time interaction ($p < 0.01$) for C_{rem} indicates that decomposition trajectories differed among communities. After one year, C_{rem} of LL was significantly lower in soil plots than in Dryas and Salix (Fig. S5). After two years, C_{rem} in Soil increased leveling out the differences between communities.

Isotopic composition of the compounds removed from LL showed a strong effect of plant community ($p < 0.01$ for N and $p < 0.05$ for C) and time ($p < 0.001$ for N and $p < 0.05$ for C), with no significant community × time interaction (Fig. S6). During the first year of decomposition, the removed compounds were consistently more isotopically depleted in soil plots, in both C and N, than in Salix or Dryas plots. Additionally, Salix showed significant differences against Soil plots, with less negative

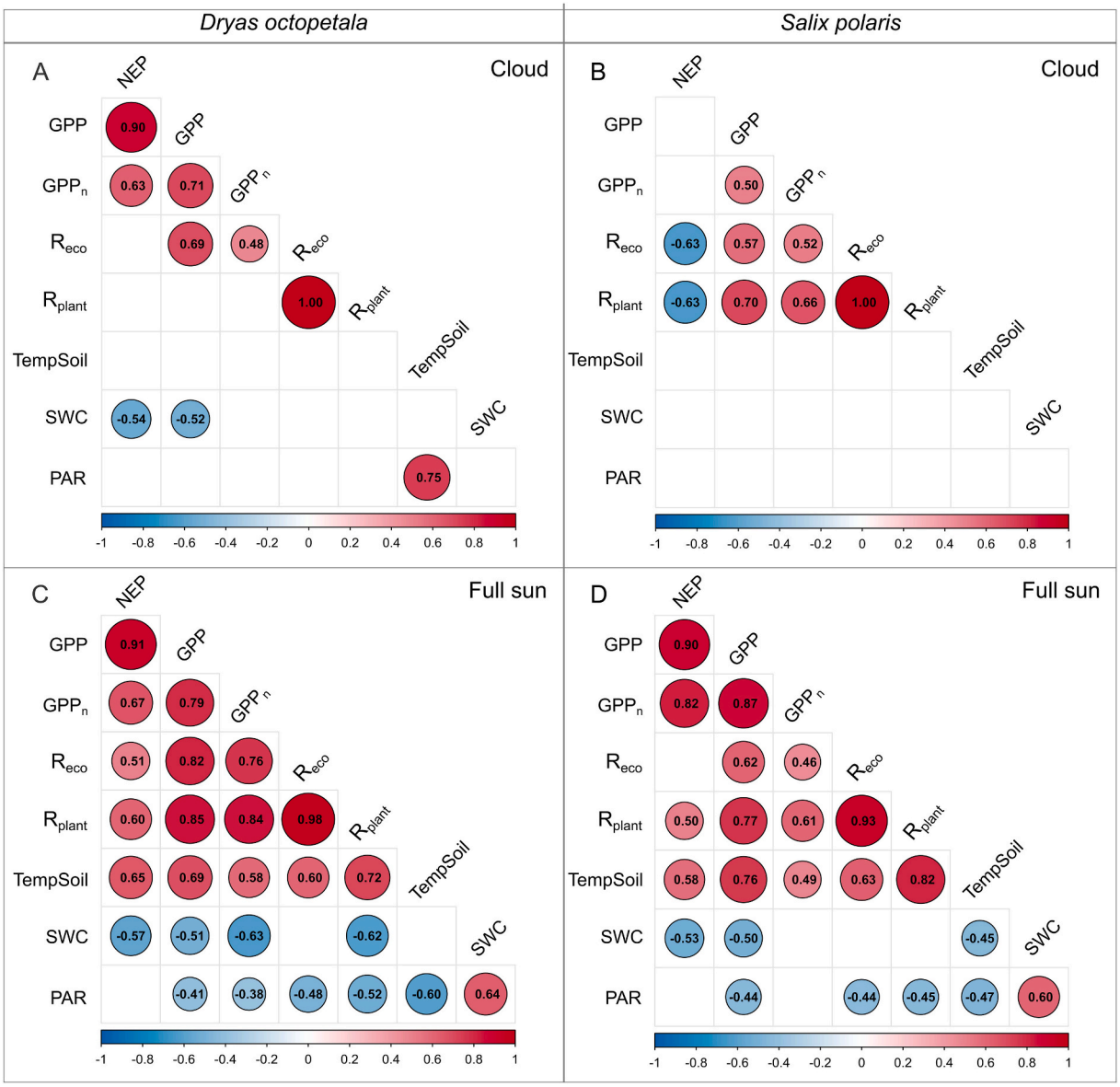


Fig. 3. Pearson correlation heatmaps of C fluxes (NEP, GPP, GPP_n, R_{eco}, R_{plant}) and environmental drivers (Soil temperature, SWC, PAR) for Dryas and Salix. Data are partitioned by weather conditions: Cloud (top row: A, B) and Full Sun (bottom row: C, D). The size and color intensity of the circles are proportional to the Pearson correlation coefficient (r). Blue circles indicate negative correlations, while red circles indicate positive correlations. Blank cells represent non-significant relationships ($p > 0.05$). Correlations were calculated using a pairwise deletion method to account for varying sample sizes across variables.

Table 3
Cell wall component and non-structural carbohydrates content (% dry weight) in the LL and RL. Values are expressed as mean ± standard error (n = 3). The effect of litter on the dependent variable was tested using a one-way analysis of variance (ANOVA). Significant differences (p-value < 0,05) are in bold.

	LL	RL	p-Value
Cell wall component content			
Ash	27.7 ± 1.26	27.01 ± 0.1	0.797
Extractives	9.12 ± 0.23	9.46 ± 0.16	0.292
Lignin	19.61 ± 0.54	43.3 ± 0.28	**2.488E^{-06}**
Cellulose	19.84 ± 0.39	9.45 ± 0.19	**1.493E^{-05}**
Hemicellulose	24.07 ± 0.51	10.75 ± 0.14	**1.439E^{-05}**
Non-structural carbohydrates content			
Starch	0.404 ± 0.055	0.274 ± 0.013	0.062
Tot. Sol	1.03 ± 0.0279	0.442 ± 0.024	**4.016E^{-06}**

values in $\delta^{13}C$ and $\delta^{15}N$ removed compounds. By the second year, communities maintained similar signatures of $\delta^{13}C$, with a significant temporal effect for Soil plots. As for $\delta^{15}N$, a significant enrichment over time of removed compounds was observed, particularly for N in Dryas and Soil plots.

3.8. Correlations - LL and RL

Decomposition constant of LL (Fig. S7, panels A, B), *k*, was positively correlated with soil respiration (Rs) ($R^2 = 0.2891$, $p < 0.05$), averaged over the two seasons. It was instead negatively correlated with $\delta^{13}C$ of SOC ($R^2 = 0.3176$, $p < 0.001$) and positively with SOC ($R^2 = 0.1746$, $p <$ 0,05). Faster decay rates were associated with greater ^{13}C mobilization from the litter in the first decomposition year. Instead, more ^{15}N has been removed from the litter in plots with higher soil C, suggesting tight coupling of C-N cycling.

In vegetated plots, remaining mass of LL after 1 year was strongly correlated with soil TN ($R^2 = 0.38$, $p < 0.01$, not shown): higher

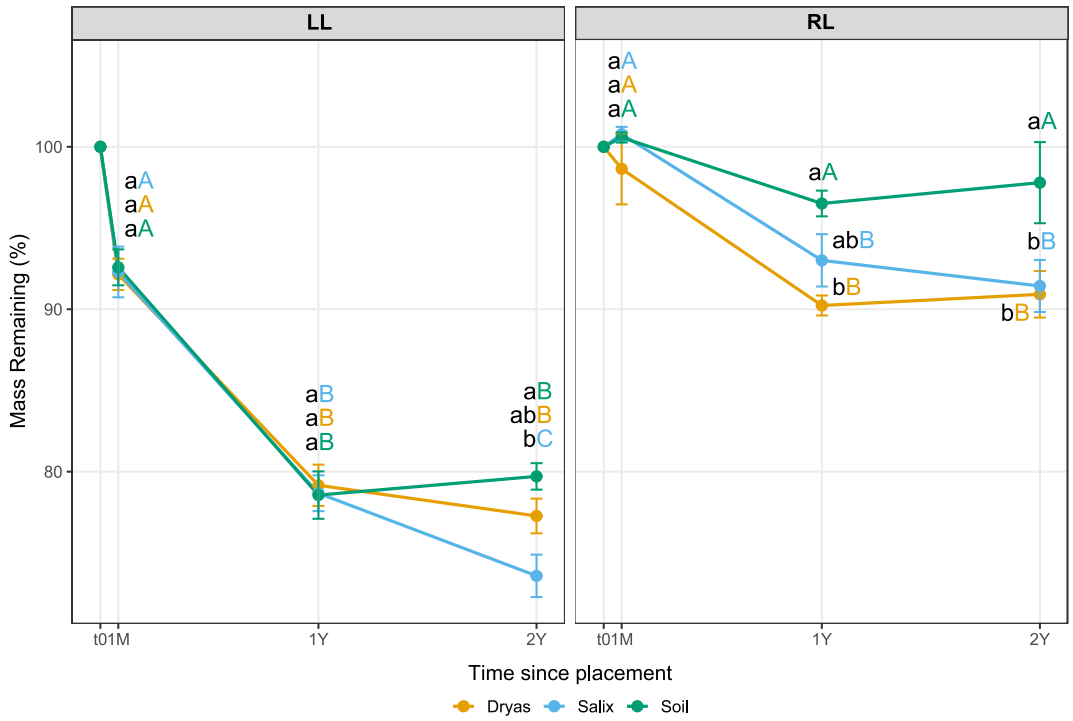


Fig. 4. Remaining mass of LL and RL litter in Dryas, Salix and Soil plots in two years of incubation. Time is expressed like 1M (1 month), 1Y (1 year) and 2Y (2 years). Black letters indicate significant differences ($p < 0.05$) between different communities in each sampling time, while colored letters indicate significant differences ($p < 0.05$) between samplings in each community (time effect inside community). A Linear Mixed Model followed by Šidák post-hoc test was applied.

decomposition occurred in plots with lower soil N. In Soil plots, this relationship was even stronger (R^2=0.73, $p < 0.05$) with a steep decline in decomposition across a very narrow gradient of soil TN. This relationship disappears after 2 years of decomposition, making k independent from TN.

For RL (Fig. S7, panels C, D), variations in the decay constant *k* were not related to any environmental variable, likely because missing values (arising from positive slopes that had to be excluded) reduced the robustness of the regression analysis. Remaining mass, however, was available for all plots and showed a clear correlation with soil N pools ($R^2 = 0.412$ with $p < 0.01$ after 1 year and $R^2 = 0.27$ with $p = 0.055$ after 2 years). Unlike LL, RL decomposition during the first year was faster in plots with higher soil N, indicating that nutrient availability stimulated the breakdown of recalcitrant material. Previous studies already highlighted interactions between litter quality and soil N availability (Knorr et al. 2005; DeMarco et al., 2014).

4. Discussion

4.1. CO_2 fluxes and drivers' relationships on multi-years perspective

Flux measurements were separated into full-sun and cloudy subsets, allowing interannual comparison despite uneven representation of light conditions among campaigns but become also particularly relevant in the High Arctic under continuous daylight, where ecosystem functioning is shaped more by transient changes in cloudiness and irradiance than by a true day-night cycle (Cannone et al., 2019; Magnani et al., 2022). Under full-sun, soil temperature was strongly associated with both assimilation and respiration in Dryas and Salix plots, consistent with the strong temperature-sensitivity of ecosystem respiration documented under experimental and natural warming in other permafrost-affected ecosystems (Qin et al., 2015). Interannual variability in GPP under full-sun, which represented the strongest pattern observed in our dataset, is consistent with the importance of temperature as a key driver of high-arctic tundra productivity (Braybrook et al., 2021). Under cloud conditions, by contrast, no measured driver significantly explained flux variation in either species, suggesting a weaker C-environmental coupling under diffuse light.

Under full-sun, higher SWC was associated with lower GPP and NEP in both Dryas and Salix, and with lower GPP_n only in Dryas, contrasting with the generally positive relationship between GPP and soil moisture reported for Arctic and dryland ecosystems (Sjögersten et al., 2006; Kannenberg et al., 2024; Magnani et al., 2022). Hence, our data do not fully support a species-specific response under high light, although two drivers were stronger predictors for NEP and GPP_n variability in Dryas. A low tolerance of wet conditions, reported for Dryas (McGraw and Antonovics, 1983) could bea possible explanation,. Under cloud conditions, SWC remained negatively associated with NEP and GPP in Dryas, but not with GPP_n, and no driver was associated with any flux in Salix. This is consistent with a weaker environmental coupling in conditions when light is the primary limiting factor.

Beyond hydrological sensitivity, the two species also differ markedly in nutrient economy. Dryas, as an evergreen dwarf shrub, reflects a conservative strategy based on longer-lived tissues and lower foliar N. In terms of access to nutrients, Dryas responds positively to cumulative precipitation. This apparent contrast with flux results suggests that seasonal (cumulative precipitation) and instantaneous (SWC) water availability regulate different processes and/or operate on different scales. Salix instead shows a more acquisitive pattern, with greater investment in N-rich tissues supported by high optical indices. It is consistent with its deciduous habit requiring faster tissue turnover and exploitation of favorable growing conditions. At the same time, Salix combined higher iWUE and lower GPP_n indicating tighter stomatal control over Dryas. This reveals a mismatch between its two strategies: an acquisitive nutrient economy paired with conservative water use, unlike Dryas, where conservative nutrient use pairs with greater photosynthetic gain. The absence of correlation between Salix fluxes and environmental drivers may reflect the relatively narrow environmental range encountered during the study. Species with tight stomatal regulation exhibit greater sensitivity of gas exchange to atmospheric water

demand, thereby decoupling C fluxes from soil moisture variation (Novick et al., 2016). Alternatively, light limitation itself may constrain the expression of other environmental responses in Salix -analogous to Liebig's law of the minimum, whereby the most limiting factor masks the influence of others regardless of their availability.

The apparent negative correlation between PAR and GPP (Fig. 3) is unlikely to indicate real photo-inhibition, as irradiance in this high-arctic context rarely exceeds the critical thresholds necessary to damage the photosynthetic apparatus (Albert et al., 2011). Instead, it likely reflects a microclimatic covariance observed during the peak vegetation window: high-irradiance conditions do not consistently correspond with optimal soil states, and frequently coincide with suboptimal thermal or hydrological conditions (Grünberg et al., 2020; von Oppen et al., 2022; Zona et al., 2023). When soil temperature and SWC are included in the models, the effect of high irradiance largely disappears, showing that under high-light conditions, soil temperature and SWC rather than irradiance are associated with C assimilation (Li et al., 2017; Magnani et al., 2022).

Reflectance indices provide further insight into the two species' different strategies. Salix exhibited consistently higher NDVI and occasionally higher G and MCARI, suggesting higher pigment pools and a greater leaf-level photosynthetic potential, consistent with eco-physiological studies reporting higher electron transport rates and energy conversion efficiency in Salix leaves compared to Dryas (Muraoka et al., 2008; Barták et al., 2012; Zagajewski et al., 2018). However, this structural leaf-level "greenness" did not translate to a proportionally higher C gain at the community scale, where Dryas maintained higher GPP, likely through an integration of water-use behavior and canopy-level traits. The PRI index, an indicator of short-term photochemical regulation and photoprotective adjustments (Gamon et al., 1992; Garbulsky et al., 2011), was constantly higher in Salix, suggesting that excess energy in Salix may be regulated more through tighter control of gas exchange, with possible additional contributions from canopy structure and its growth within moss-lichen cushions. In Dryas, the more negative PRI is consistent with stronger engagement of photoprotective pathways, which may help sustain the comparatively high GPP observed for this species. These patterns highlight the species-specific plasticity that characterizes Arctic shrubs across different biomes (Myers-Smith et al., 2015; Wang and Wen, 2022).

4.2. Physiological and resource-use strategies

The spectral and photoprotective differences are directly reflected in the species' leaf biochemistry (Fig. 2E). The conservative nature of the evergreen Dryas is confirmed by its consistently higher C:N ratio and lower foliar N content, indicating a substantial C allocation to cell-wall structural compounds for effective nutrient retention (López-Blanco et al., 2020; Zibulski et al., 2017). Conversely, the acquisitive strategy of the deciduous Salix is sustained by its significant investment in N-rich tissues, which supports higher potential C assimilation (Muraoka et al., 2002). Although these biochemical differences between the two species were consistent across most of the study period, the lack of significant differences in foliar nutrients observed in 2022 suggests that year-to-year environmental variations - such as shifts in precipitation, soil thaw depth, or localized animal inputs - can modulate how strongly these species-specific physiological strategies are expressed, even though their fundamental functional traits remain distinct (Betway et al., 2021; Saccone et al., 2017).

The different photosynthetic and water-use strategies were supported by isotopic data. The lower iWUE and higher c_i/c_a coupled to higher GPP in Dryas are consistent with higher stomatal conductance. As suggested by Welker et al. (1993), this behavior in Dryas reflects flexibility in water-use regulation, with plant adopting a less conservative water-use strategy and ensures C gain under local relatively dry well drained soil conditions. On the other hand, higher iWUE of Salix indicates stomatal constraints under similar conditions pointing on conservative strategy with greater control over gas exchange (Wang and Wen, 2022).

The $\delta^{15}N$ patterns of leaf tissues were more variable and less species-specific, implying that both Dryas and Salix access similar N sources. The higher $\delta^{15}N$ values observed in Salix in 2021 may reflect a transient increase in the availability of ^{15}N-enriched inorganic N pools from microbial mineralization (Ramm et al., 2022), surface deposition (Choudhary et al., 2016) or animal input (Van Der Wal et al., 2004), but the lack of consistent trends across years suggests that the N cycle in these high-arctic soils is highly dynamic and spatially heterogeneous.

4.3. Impact of shrubs on soil characteristics and activity

Compared with bare soil, plots colonized by vascular plants contained larger soil C and N, although the statistical pattern differed between the two variables (Tab. 2). The higher stocks are consistent with the role of vegetation as the main source of organic matter inputs to tundra soils, enhancing C sequestration and nutrient accumulation through above- and belowground biomass production (Chapin et al., 2011). Furthermore, *D. octopetala* is known to form symbiotic associations with N-fixing bacteria Frankia, which may contribute to local increase in N concentrations (Apple et al., 2019). However, the similar foliar $\delta^{15}N$ between Dryas and Salix do not provide direct evidence for enhanced N fixation relative to *Salix*-dominated plots. The lack of statistically significant differences in soil C and N pools between Dryas- and Salix-dominated microsites indicates that despite potential differences in productivity, litter inputs, rhizosphere processes, and decomposition dynamics, C and N inputs and losses were broadly balanced, resulting in similar soil pools over time. The absence of differences in soil $\delta^{15}N$ across all three communities further suggests no strong, persistent divergence in dominant N sources or in N-cycling openness at the bulk-soil scale, whereas the more negative $\delta^{13}C$ of vegetated soils relative to bare patches is consistent with a larger contribution from plant-derived organic matter and/or less processed organic material.

Microbial community functioning in shrub communities and bare soil patches was assessed through the decomposition experiment. Decomposition of LL in year 1 resulted in similar biomass loss across vegetated and bare soil plots; however, the nature of the compounds removed differed among communities, as indicated by distinct $\delta^{13}C$ and $\delta^{15}N$ signatures of C and N lost and by differential % of remaining C. During decomposition process, litter C can follow multiple pathways - leaching into the soil at early phases, incorporation into microbial biomass, transformation into simpler organic compounds and eventual mineralization to CO_2 (Cotrufo et al., 2015; DeMarco et al., 2014)- with non-structural soluble compounds typically lost first as the most accessible for microbial community and leaching process (Berg and McClaugherty, 2008). Because vegetation cover creates strong spatial variation in microclimate in tundra ecosystems (von Oppen et al., 2022), leaching dynamics are expected to differ between bare soil and vegetated microsites. Moss-shrub (Salix) and shrub (Dryas) cushions provide thermal insulation and stabilize moisture regimes (Gonzalez Martinez et al., 2026; Gornall et al., 2007), which buffer soil moisture fluctuations and regulate water flow. Such buffering would reduce the mobility of soluble, isotopically lighter compounds released from LL. In contrast, bare soil plots experience faster drainage and greater early loss of dissolved organic C and N. If soil temperature is indeed higher in bare patches, this would further accelerate leaching and microbial use of labile substrates in these plots (Blok et al., 2018; Xue et al., 2016).

Beyond physically driven fractionation, differences in microbial substrate use may also have contributed to the observed $\delta^{13}C$ and $\delta^{15}N$ patterns, though microbial functional diversity was not assessed in this study. The more stable isotopic trajectories in vegetated plots are consistent with a rhizosphere-influenced decomposer community, while decomposition in bare soil appears dominated by lability gradients alone. The pronounced time effect for $\delta^{15}N$ in Dryas plots likely reflects the influence of phenolic-rich RL litter, which increases microbial N

demand during decomposition. The absence of a clear $\delta^{15}N$ shift in Salix plots may be related to its growth within moss-lichen cushions, which regulate microclimate and water fluxes (Bueno et al., 2016; Jaroszynska et al., 2023), and intercept atmospheric and animal-derived N inputs (Barthelemy et al., 2024) potentially altering microbial N use relative to Dryas (Koranda and Michelsen, 2021) - consistent with LL decomposition in Salix plots not reaching a steady state within the two-year study, unlike in Dryas and Soil plots.

Litter quality was the strongest determinant of decomposition dynamics in this experiment. RL exhibited markedly slower early decomposition which is congruent with lower content of total soluble content (Tab. 3) and with the accessibility of these compounds being strongly constrained by litter structural properties such as lignification, tissue toughness, and polyphenolic protection. Indeed, lignin, which was present at higher concentrations in RL, is the most recalcitrant component to microbial degradation in litter and acts as a key inhibitor of decomposition (Berg, 2000; Gartner and Cardon, 2004), consistent with soil organic matter quality models showing systematic differences in decomposability among tundra vegetation cover types (Andersen and White, 2006).

The increase in N_{rem} observed in RL over time reflects the preferential loss of C-rich components, causing a relative enrichment of N-containing compounds in the residual material. This pattern is characteristic of low-quality, lignin- and polyphenol-rich dwarf shrub litter, such as Dryas (Aerts et al., 2003; DeMarco et al., 2014; Hobbie, 1996). High polyphenol levels can form stable N-binding complexes (Cornelissen et al., 2007; Gallardo and Merino, 1992), slowing N release and producing apparent N retention. With ongoing shrub expansion in the Arctic, this enhanced N retention in recalcitrant shrub litter may further concentrate N cycling beneath shrubs while reducing N availability in open areas, increasing fine-scale nutrient heterogeneity.

Plant community effects on decomposition emerged earlier for RL than for LL and became more pronounced over time, with the slowest decay of RL consistently observed in the Soil plots. This suggests that colonization by vascular plants and the associated rhizosphere fundamentally alter the capacity to decompose structurally complex substrates - potentially through root exudation, rhizosphere priming, and shifts in microbial community composition (Tejnecký et al., 2025; Friggens et al., 2025; Hartmann et al., 2009) - though these specific mechanisms were not measured directly and would require targeted investigation. Considering these complex plant-soil interactions in ecosystem models is thus crucial for accurately forecasting C-nutrient-climate feedbacks in rapidly changing Arctic.

5. Conclusion

This study shows that C exchange in high-arctic shrub communities is shaped by the interactions among light conditions, environmental variability and species-specific functional strategies. Under full-sun conditions, soil temperature emerged as an important factor associated with C fluxes. Under cloudy conditions, associations between C fluxes and environmental variables were weaker, limited to SWC in Dryas, suggesting that light limitation constrains temperature- and moisture-related responses. The two species differed markedly in nutrient economy and water-use strategy, with consequences for plot-scale C uptake and nutrient cycling. Salix was characterized by a more acquisitive nutrient-use strategy; however, this trait did not translate into greater community- and leaf-scale C gain likely due to the combination with conservative water use. Conversely, Dryas combined a conservative nutrient economy, associated with its evergreen habit, with a less conservative water-use strategy and stronger realized photosynthetic performance. Under full-sun conditions, increasing SWC was also associated with lower ecosystem C gain in both communities, and with lower GPP_n in Dryas only, a pattern that warrants further investigation; consequences for annual C-sink capacity cannot be inferred from the present peak-season measurements. Vegetated microsites also supported greater processing of structurally complex litter than bare soil, although the magnitude and timing of this effect varied with litter type and shrub community. Recognizing this functional diversity among high-arctic shrub communities is therefore important for improving predictions of C-nutrient-climate feedbacks in a rapidly changing Arctic.

Declaration of generative AI and AI-assisted technologies in the manuscript preparation process

During the preparation of this work, the authors used Gemini Pro to refine the language, style, and readability of the text. The authors reviewed and edited the output as needed and take full responsibility for the content of the published article.

CRediT authorship contribution statement

Carlotta Volterrani: Writing – original draft, Visualization, Investigation, Formal analysis, Data curation. **Angela Augusti:** Supervision, Project administration, Methodology, Funding acquisition. **Enrico Brugnoli:** Writing – review & editing. **Federica D'Alò:** Writing – review & editing, Investigation. **Stefano Moscatello:** Writing – review & editing, Investigation. **Emanuele Pallozzi:** Writing – review & editing, Supervision, Resources, Investigation. **Olga Gavrichkova:** Writing – review & editing, Supervision, Resources, Project administration, Methodology, Investigation.

Funding sources

This work was supported by the Research Council of Norway, grant n° 291644 [SIOS 2017_0009 "Contribution of Vegetation and Soil components to Carbon cycle in Arctic environment in relationship to climate change" (VegSoCa) and SIOS Access Call 2019 "Effects of big herbivores on the functioning of decomposers and primary producers in High Arctic tundra" (GrazeAct)], Svalbard Integrated Arctic Earth Observing System - Knowledge Centre (SIOS-KC).

Declaration of competing interest

The authors declare the following financial interests/personal relationships which may be considered as potential competing interests: co-author Dr. Olga Gavrichkova, given her role as guest editor, had no involvement in the peer review of this article and had no access to information regarding its peer review. Full responsibility for the editorial process for this article was delegated to another journal editor If there are other authors, they declare that they have no known competing financial interests or personal relationships that could have appeared to influence the work reported in this paper.

Acknowledgements

Authors would like to express their sincere thanks to Luciano Spaccino and Irene Tunno for their assistance in elemental and stable isotope analyses, to trainee students Alessia Nardecchia, Gianluca Mancinelli, Giulia Onnelli and Chiara Immordino for their support in sampling preparation and classification, to Massimiliano Vardè, Marco Casula, Ombretta Dell'Acqua, Simonetta Montaguti, Tessa Viglezio and all the management staff of the CNR Arctic Research Base "Dirigibile Italia" in Ny-Ålesund, Svalbard, who made this work possible. Authors sincerely thank the reviewers for their critical reading and helpful comments, which guided us in refining the presentation of our findings. This work is dedicated to the memory of our friend and colleague, Angela Augusti, whose foundational research and initial insights made this project possible.

Appendix A. Supplementary data

Supplementary data to this article can be found online at https://doi.org/10.1016/j.coldregions.2026.105203

Data availability

The datasets are available as supplementary material and stored in the Italian Arctic Data Center (IADC) repository at the following links: https://doi.org/10.71761/27b5e41a-898d-4d08-a86f-02dade483462, https://doi.org/10.71761/0bff91f8-c083-4ff8-a3cd-bc3f4dbf11c8, https://doi.org/10.71761/e6bbba58-fa41-420b-8d34-e11940408178, https://doi.org/10.71761/ae3bf3b0-b275-4166-bb91-71c7bd383718.

References

Aerts, R., De Caluwe, H., Beltman, B., 2003. Plant community mediated vs. nutritional controls on litter decomposition rates in grasslands. Ecology 84 (12), 3198–3208. https://doi.org/10.1890/02-0712.

Albert, K.R., Mikkelsen, T.N., Ro-Poulsen, H., Arndal, M.F., Michelsen, A., 2011. Ambient UV-B radiation reduces PSII performance and net photosynthesis in high Arctic Salix arctica. Environ. Exp. Bot. 72 (3), 439–447. https://doi.org/10.1016/j.envexpbot.2010.07.001.

Andersen, S.K., White, D.M., 2006. Determining soil organic matter quality under anaerobic conditions in arctic and subarctic soils. Cold Reg. Sci. Technol. 44 (2), 149–158. https://doi.org/10.1016/j.coldregions.2005.11.001.

Apple, M.E., Ricketts, M.K., Martin, A.C., 2019. Plant functional traits and microbes vary with position on striped periglacial patterned ground at Glacier National Park, Montana. J. Geogr. Sci. 29 (7), 1127–1141. https://doi.org/10.1111/geb.13512.

Barták, M., Váczi, P., Hájek, J., 2012. Photosynthetic activity in three vascular species of Spitsbergen vegetation during summer season in response to microclimate. Polish Polar Res. 33 (4), 443–462. https://doi.org/10.2478/v10183−012−0018−z.

Barthelemy, H., Nobel, L.A., Stark, S., Väisänen, M., Olofsson, J., Michelsen, A., 2024. Short- and long-term plant and microbial uptake of 15N-labelled urea in a mesic tundra heath, West Greenland. Polar Biol. 47 (1), 1–15. https://doi.org/10.1007/s00300-023-03209-6.

Bartoń, K., 2026. MuMIn: Multi-Model Inference; R Package Version 1.48.19. https://CRAN.R-project.org/package=MuMIn.

Bates, D., Mächler, M., Bolker, B., Walker, S., 2015. Fitting linear mixed-effects models using lme4. J. Stat. Softw. 67 (1). https://doi.org/10.18637/jss.v067.i01.

Berg, B., 2000. Litter decomposition and organic matter turnover in northern forest soils. For. Ecol. Manag. 133 (1–2), 13–22. https://doi.org/10.1016/S0378-1127(99)00294-7.

Berg, B., McClaugherty, C., 2008. Chemical constituents as rate-regulating: initial variation and changes during decomposition. In: Berg, B., McClaugherty, C. (Eds.), Plant Litter: Decomposition, Humus Formation, Carbon Sequestration. Springer, Berlin Heidelberg, pp. 115–148. https://doi.org/10.1007/978-3-540-74923-3_6.

Betway, K.R., Hollister, R.D., May, J.L., Oberbauer, S.F., 2021. Species-specific trends and variability in plant functional traits across a latitudinal gradient in northern Alaska. J. Veg. Sci. 32 (3). https://doi.org/10.1111/jvs.13040.

Blok, D., Faucherre, S., Banyasz, I., Rinnan, R., Michelsen, A., Elberling, B., 2018. Contrasting above- and belowground organic matter decomposition and carbon and nitrogen dynamics in response to warming in High Arctic tundra. Glob. Chang. Biol. 24 (6), 2660–2672. https://doi.org/10.1111/gcb.14017.

Boike, J., Grünberg, I., Miesner, F., Bornemann, N., Cable, W.L., 2022. Continuous measurements in soil and air at the permafrost long-term observatory at the Bayelva station near Ny-Ålesund (2018 et seq). PANGAEA. https://doi.org/10.1594/PANGAEA.948951.

Braybrook, C.A., Scott, N.A., Treitz, P.M., Humphreys, E.R., 2021. Interannual variability of summer net ecosystem CO2 exchange in high Arctic Tundra. J. Geophys. Res. Biogeosci. 126 (8). https://doi.org/10.1029/2020JG006094.

Bueno, C.G., Williamson, S.N., Barrio, I.C., Helgadóttir, Á., HiK, D.S., 2016. Moss mediates the influence of shrub species on soil properties and processes in alpine tundra. PLoS One 11 (10), e0164143. https://doi.org/10.1371/journal.pone.0164143.

Cannone, N., Augusti, A., Malfasi, F., Pallozzi, E., Calfapietra, C., Brugnoli, E., 2016. The interaction of biotic and abiotic factors at multiple spatial scales affects the variability of CO2 fluxes in polar environments. Polar Biol. 39 (9), 1581–1596. https://doi.org/10.1007/s00300-015-1883-9.

Cannone, N., Ponti, S., Christiansen, H.H., Christensen, T.R., Pirk, N., Guglielmin, M., 2019. Effects of active layer seasonal dynamics and plant phenology on CO2 land-atmosphere fluxes at polygonal tundra in the High Arctic, Svalbard. CATENA 174, 142–153. https://doi.org/10.1016/j.catena.2018.11.013.

Chae, Y., Kang, S.M., Jeong, S.J., Kim, B., Frierson, D.M.W., 2015. Arctic greening can cause earlier seasonality of Arctic amplification. Geophys. Res. Lett. 42 (2), 536–541. https://doi.org/10.1002/2014GL061841.

Chapin, F. Stuart, Vitousek Peter, M., Matson Pamela, A., 2011. Principles of Terrestrial Ecosystem Ecology. https://doi.org/10.1007/978-1-4419-9504-9.

Choudhary, S., Blaud, A., Osborn, A.M., Press, M.C., Phoenix, G.K., 2016. Nitrogen accumulation and partitioning in a High Arctic tundra ecosystem from extreme atmospheric N deposition events. Sci. Total Environ. 554–555, 303–310. https://doi.org/10.1016/j.scitotenv.2016.02.155.

Copernicus Sentinel-2 (processed by ESA), 2022. Sentinel-2 MSI Level-2A BOA reflectance. In: Sentinel-2 MSI Level-2A BOA Reflectance. https://doi.org/10.5270/S2_-znk9xsj.

Cornelissen, J.H.C., Van Bodegom, P.M., Aerts, R., Callaghan, T.V., Van Logtestijn, R.S.P., Alatalo, J., Stuart Chapin, F., Gerdol, R., Gudmundsson, J., Gwynn-Jones, D., Hartley, A.E., Hik, D.S., Hofgaard, A., Jónsdóttir, I.S., Karlsson, S., Klein, J.A., Laundre, J., Magnusson, B., Michelsen, A., Zhao, X., 2007. Global negative vegetation feedback to climate warming responses of leaf litter decomposition rates in cold biomes. Ecol. Lett. 10 (7), 619–627. https://doi.org/10.1111/j.1461-0248.2007.01051.x.

Cotrufo, M.F., Soong, J.L., Horton, A.J., Campbell, E.E., Haddix, M.L., Wall, D.H., Parton, W.J., 2015. Formation of soil organic matter via biochemical and physical pathways of litter mass loss. Nat. Geosci. 8 (10), 776–779. https://doi.org/10.1038/ngeo2520.

Cowan, I.R.L., 1986. Economics of Carbon Fixation in Higher Plants. https://api.semanticscholar.org/CorpusID:127844839.

Daughtry, C., Walthall, C.L., Kim, M.S., Brown de Colstoun, E., McMurtrey III, J.E., 2000. Estimating corn leaf chlorophyll concentration from leaf and canopy reflectance. Remote Sens. Environ. 74 (2), 229–239. https://doi.org/10.1016/S0034-4257(00)00113-9.

DeMarco, J., Mack, M.C., Bret-Harte, M.S., 2014. Effects of arctic shrub expansion on biophysical vs. biogeochemical drivers of litter decomposition. Ecology 95 (7), 1861–1875. https://doi.org/10.1890/13-2221.1.

Dudley, S.A., 1996. Differing selection on plant physiological traits in response to environmental water availability: a test of adaptive hypotheses. Evolution 50 (1), 92–102. https://doi.org/10.1111/j.1558-5646.1996.tb04475.x.

Elmendorf, S.C., Henry, G.H.R., Hollister, R.D., Björk, R.G., Boulanger-Lapointe, N., Cooper, E.J., Cornelissen, J.H.C., Day, T.A., Dorrepaal, E., Elumeeva, T.G., Gill, M., Gould, W.A., Harte, J., Hik, D.S., Hofgaard, A., Johnson, D.R., Johnstone, J.F., Jónsdóttir, I.S., Jorgenson, J.C., Wipf, S., 2012. Plot-scale evidence of tundra vegetation change and links to recent summer warming. Nat. Clim. Chang. 2 (6), 453–457. https://doi.org/10.1038/nclimate1465.

Farquhar, G.D., O'leary, M.H., Berry, J.A., 1982. On the relationship between carbon isotope discrimination and the intercellular carbon dioxide concentration in leaves. Aust. J. Plant Physiol. 9. https://doi.org/10.1071/PP9820121.

Farquhar, G.D., Richards, R.A., 1984. Isotopic composition of plant carbon correlates with water-use efficiency of wheat genotypes. Aust. J. Plant Physiol. 11 (6), 539–552. https://doi.org/10.1071/PP9840539.

Fox, J., & Weisberg, S. (2019). An R Companion to Applied Regression, Third ed. (Sage, ISBN: 9781412975148.

Friggens, N.L., Hugelius, G., Kokelj, S.V., Murton, J.B., Phoenix, G.K., Hartley, I.P., 2025. Positive rhizosphere priming accelerates carbon release from permafrost soils. Nat. Commun. 16 (1). https://doi.org/10.1038/s41467-025-58845-9.

Gallardo, A., Merino, J., 1992. Nitrogen immobilization in leaf litter at two Mediterranean ecosystems of SW Spain. Biogeochemistry 15. https://doi.org/10.1007/BF00002937.

Gamon, J.A., Peñuelas, J., Field, C.B., 1992. A narrow-waveband spectral index that tracks diurnal changes in photosynthetic efficiency. Remote Sens. Environ. 41 (1), 35–44. https://doi.org/10.1016/0034-4257(92)90059-S.

Gamon, J.A., Serrano, L., Surfus, J.S., 1997. The photochemical reflectance index: an optical indicator of photosynthetic radiation use efficiency across species, functional types, and nutrient levels. Oecologia 112, 492–501. https://doi.org/10.1007/s004420050337.

Garbulsky, M.F., Peñuelas, J., Gamon, J., Inoue, Y., Filella, I., 2011. The photochemical reflectance index (PRI) and the remote sensing of leaf, canopy and ecosystem radiation use efficiencies: a review and meta-analysis. Remote Sens. Environ. 115 (2), 281–297. https://doi.org/10.1016/j.rse.2010.08.023.

Gartner, T.B., Cardon, Z.G., 2004. Decomposition dynamics in mixed-species leaf litter. Oikos 104 (2), 230–246. https://doi.org/10.1111/j.0030-1299.2004.12738.x.

Gavrichkova, O., Brykova, R.A., Brugnoli, E., Calfapietra, C., Cheng, Z., Kuzyakov, Y., Liberati, D., Moscatelli, M.C., Pallozzi, E., Vasenev, V.I., 2020. Secondary soil salinization in urban lawns: Microbial functioning, vegetation state, and implications for carbon balance. Land Degrad. Dev. 31 (17), 2591–2604. https://doi.org/10.1002/ldr.3627.

Gonzalez Martinez, K.J., Zona, D., Biggs, T., Bernabe, K., Sirivat, D., Tenorio, F., Oechel, W., 2026. Influences of the moss layer and environmental drivers on the active layer depth and soil temperature in a wet sedge Arctic tundra ecosystem. Environ. Res. Ecol. 5 (1), 015001. https://doi.org/10.1088/2752-664X/ae212b.

Gornall, J.L., Jónsdóttir, I.S., Woodin, S.J., Van der Wal, R., 2007. Arctic mosses govern below-ground environment and ecosystem processes. Oecologia 153 (4), 931–941. https://doi.org/10.1007/s00442-007-0785-0.

Grünberg, I., Miesner, F., Bornemann, N., Cable, W.L., Boike, J., 2025. Meteorological and soil data from Bayelva, Svalbard, homogenised data product (version 2: 1998-09-13 to 2024-12-31, design 1: database). PANGAEA. https://doi.org/10.1594/PANGAEA.981132.

Grünberg, I., Wilcox, E.J., Zwieback, S., Marsh, P., Boike, J., 2020. Linking tundra vegetation, snow, soil temperature, and permafrost. Biogeosciences 17 (16), 4261–4279. https://doi.org/10.5194/bg-17-4261-2020.

Hair, J.F., Babin, B.J., Anderson, R.E., Black, W.C., 2019. Multivariate Data Analysis, (8th ed.). Cengage Learning https://www.cengage.uk/c/multivariate-data-analysis-8e-hair-babin-anderson-black/9781473756540/?searchIsbn=9781473756540.

Hartmann, A., Schmid, M., van Tuinen, D., Berg, G., 2009. Plant-driven selection of microbes. Plant Soil 321 (1–2), 235–257. https://doi.org/10.1007/s11104-008-9814-y.

Hobbie, S.E., 1996. Temperature and plant species control over litter decomposition in Alaskan Tundra. Ecol. Monogr. 66 (4), 503–522. https://doi.org/10.2307/2963492.
Isaksen, K., Nordli, Ø., Ivanov, B., Køltzow, M.A.Ø., Aaboe, S., Gjelten, H.M., Mezghani, A., Eastwood, S., Førland, E., Benestad, R.E., Hanssen-Bauer, I., Brækkan, R., Sviashchennikov, P., Demin, V., Revina, A., Karandasheva, T., 2022. Exceptional warming over the Barents area. Sci. Rep. 12 (1). https://doi.org/10.1038/s41598-022-13568-5.
Jaroszynska, F., Althuizen, I., Halbritter, A.H., Klanderud, K., Lee, H., Telford, R.J., Vandvik, V., 2023. Bryophytes dominate plant regulation of soil microclimate in alpine grasslands. Oikos 2023 (12). https://doi.org/10.1111/oik.10091.
Kannenberg, S.A., Anderegg, W.R.L., Barnes, M.L., Dannenberg, M.P., Knapp, A.K., 2024. Dominant role of soil moisture in mediating carbon and water fluxes in dryland ecosystems. Nat. Geosci. 17 (1), 38–43. https://doi.org/10.1038/s41561-023-01351-8.
Karlsen, S.R., Elvebakk, A., Høgda, K.A., Grydeland, T., 2014. Spatial and temporal variability in the onset of the growing season on svalbard, arctic Norway - measured by MODIS-NDVI satellite data. Remote Sens. 6 (9), 8088–8106. https://doi.org/10.3390/rs6098088.
Karlsen, S.R., Elvebakk, A., Stendardi, L., Høgda, K.A., Macias-Fauria, M., 2024. Greening of Svalbard. Sci. Total Environ. 945. https://doi.org/10.1016/j.scitotenv.2024.174130.
Karlsen, S.R., Elvebakk, A., Tømmervik, H., Belda, S., Stendardi, L., 2022. Changes in onset of vegetation growth on Svalbard, 2000–2020. Remote Sens. 14 (24). https://doi.org/10.3390/rs14246346.
Koranda, M., Michelsen, A., 2021. Mosses reduce soil nitrogen availability in a subarctic birch forest via effects on soil thermal regime and sequestration of deposited nitrogen. J. Ecol. 109 (3), 1424–1438. https://doi.org/10.1111/1365-2745.13567.
Kottek, M., Grieser, J., Beck, C., Rudolf, B., Rubel, F., 2006. World map of the Köppen-Geiger climate classification updated. Meteorol. Z. 15 (3), 259–263. https://doi.org/10.1127/0941-2948/2006/0130.
Kuzyakov, Y., 2006. Sources of CO2 efflux from soil and review of partitioning methods. Soil Biol. Biochem. 38 (3), 425–448. https://doi.org/10.1016/j.soilbio.2005.08.020.
Kuzyakov, Y., Gavrichkova, O., 2010. Time lag between photosynthesis and carbon dioxide efflux from soil: a review of mechanisms and controls. Glob. Chang. Biol. 16 (12), 3386–3406. https://doi.org/10.1111/j.1365-2486.2010.02179.x.
Lafleur, P.M., Campeau, A.B., Kang, S., 2020. Carbon dioxide fluxes of tundra vegetation communities on an esker top in the low-arctic. Adv. Polar Sci. 31 (3), 167–177. https://doi.org/10.13679/j.advps.2020.0017.
Lenth, R.V., Piaskowski, J., 2026. emmeans: Estimated Marginal Means, aka Least-Squares Means. Https://Rvlenth.Github.Io/Emmeans/. https://rvlenth.github.io/emmeans/.
Li, F., Zhu, R., Tao, B., Wang, Q., Hua, Xu, 2017. Summertime CO 2 fluxes from tundra of Ny-Ålesund in the High Arctic. High Arctic. Adv Polar Sci 28 (1), 50–60. https://doi.org/10.13679/j.advps.2017.1.00050.
López-Blanco, E., Jackowicz-Korczynski, M., Mastepanov, M., Skov, K., Westergaard-Nielsen, A., Williams, M., Christensen, T.R., 2020. Multi-year data-model evaluation reveals the importance of nutrient availability over climate in arctic ecosystem C dynamics. Environ. Res. Lett. 15 (9). https://doi.org/10.1088/1748-9326/ab865b.
Magnani, M., Baneschi, I., Giamberini, M., Raco, B., Provenzale, A., 2022. Microscale drivers of summer CO2 fluxes in the Svalbard High Arctic tundra. Sci. Rep. 12 (1). https://doi.org/10.1038/s41598-021-04728-0.
Maturilli, M., 2020. Continuous meteorological observations at station Ny-Ålesund (2011-08 et seq). PANGAEA. https://doi.org/10.1594/PANGAEA.914979.
McGraw, J.B., Antonovics, J., 1983. Experimental ecology of Dryas octopetala ecotypes: I. Ecotypic differentiation and life-cycle stages of selection. J. Ecol. 879–897. https://doi.org/10.2307/2259599.
Midwood, A.J., Boutton, T.W., 1998. Soil carbonate decomposition by acid has little effect on δ13C of organic matter. Soil Biol. Biochem. 30 (10–11), 1301–1307. https://doi.org/10.1016/S0038-0717(98)00030-3.
Moscatello, S., Proietti, S., Augusti, A., Scartazza, A., Walker, R.P., Famiani, F., Battistelli, A., 2017. Late summer photosynthesis and storage carbohydrates in walnut (Juglans regia L.): feed-back and feed-forward effects. Plant Physiol. Biochem. 118, 618–626. https://doi.org/10.1016/j.plaphy.2017.07.025.
Muraoka, H., Noda, H., Uchida, M., Ohtsuka, T., Koizumi, H., Nakatsubo, T., 2008. Photosynthetic characteristics and biomass distribution of the dominant vascular plant species in a high Arctic tundra ecosystem, Ny-Ålesund, Svalbard: implications for their role in ecosystem carbon gain. J. Plant Res. 121 (2), 137–145. https://doi.org/10.1007/s10265-007-0134-8.
Muraoka, H., Uchida, M., Mishio, M., Nakatsubo, T., Kanda, H., Koizumi, H., 2002. Leaf photosynthetic characteristics and net primary production of the polar willow (Salix polaris) in a high arctic polar semi-desert, Ny-Ålesund, Svalbard. Can. J. Bot. 80 (11), 1193–1202. https://doi.org/10.1139/b02-108.
Myers-Smith, I., Forbes, B., Wilmking, M., Hallinger, M., Lantz, T., Blok, D., Tape, K., Macias-Fauria, M., Sass-Klaassen, U., Lévesque, Es, Boudreau, S., Ropars, P., Hermanutz, L., Trant, A., Siegwart Collier, L., Weijers, S., Rozema, J., Rayback, S., Schmidt, N., Hik, D., 2011. Shrub expansion in tundra ecosystems: dynamics, impacts and research priorities. Environ. Res. Lett. 6, 045509. https://doi.org/10.1088/1748-9326/6/4/045509.
Myers-Smith, I.H., Elmendorf, S.C., Beck, P.S.A., Wilmking, M., Hallinger, M., Blok, D., Tape, K.D., Rayback, S.A., Macias-Fauria, M., Forbes, B.C., Speed, J.D.M., Boulanger-Lapointe, N., Rixen, C., Lévesque, E., Schmidt, N.M., Baittinger, C., Trant, A.J., Hermanutz, L., Collier, L.S., Vellend, M., 2015. Climate sensitivity of shrub growth across the tundra biome. Nat. Clim. Chang. 5 (9), 887–891. https://doi.org/10.1038/nclimate2697.
Novick, K., Ficklin, D., Stoy, P., Williams, C.A., Bohrer, G., Christopher Oishi, A., Papuga, S.A., Blanken, P.D., Noormets, A., Sulman, B.N., Scott, R.L., Wang, L., Phillips, R.P., 2016. The increasing importance of atmospheric demand for ecosystem water and carbon fluxes. Nat. Clim. Chang. 6, 1023–1027. https://doi.org/10.1038/nclimate3114.
Panshin, A.J., de Zeeuw, C., 1980. Textbook of wood technology. Open J. For. 5 (5).
Parker, T.C., Sanderman, J., Holden, R.D., Blume-Werry, G., Sjögersten, S., Large, D., Castro-Díaz, M., Street, L.E., Subke, J., Wookey, P.A., 2018. Exploring drivers of litter decomposition in a greening Arctic: results from a transplant experiment across a treeline. Ecology 99 (10), 2284–2294. https://doi.org/10.1002/ecy.2442.
Portarena, S., Farinelli, D., Famiani, F., Cinosi, N., Traini, C., Rezaei, N., Brugnoli, E., 2024. Differential tolerance to summer stress conditions in two olive cultivars using the dendro-isotopic approach. Dendrochronologia 84. https://doi.org/10.1016/j.dendro.2024.126182.
Previdi, M., Janoski, T.P., Chiodo, G., Smith, K.L., Polvani, L.M., 2020. Arctic amplification: a rapid response to radiative forcing. Geophys. Res. Lett. 47 (17). https://doi.org/10.1029/2020GL089933.
Pushkareva, E., Johansen, J.R., Elster, J., 2016. A review of the ecology, ecophysiology and biodiversity of microalgae in Arctic soil crusts. In: Polar Biology, vol. 39. Springer Verlag, pp. 2227–2240. https://doi.org/10.1007/s00300-016-1902-5. Number 12.
Qin, Y., Yi, S., Chen, J., Ren, S., Wang, X., 2015. Responses of ecosystem respiration to short-term experimental warming in the alpine meadow ecosystem of a permafrost site on the Qinghai–Tibetan Plateau. Cold Reg. Sci. Technol. 115, 77–84. https://doi.org/10.1016/j.coldregions.2015.03.012.
R Core Team, 2025. R: A Language and Environment for Statistical Computing. R Foundation for Statistical Computing. https://www.r-project.org/.
Ramm, E., Liu, C., Ambus, P., Butterbach-Bahl, K., Hu, B., Martikainen, P.J., Marushchak, M.E., Mueller, C.W., Rennenberg, H., Schloter, M., Siljanen, H.M.P., Voigt, C., Werner, C., Biasi, C., Dannenmann, M., 2022. A review of the importance of mineral nitrogen cycling in the plant-soil-microbe system of permafrost-affected soils—changing the paradigm. Environ. Res. Lett. 17 (1), 013004. https://doi.org/10.1088/1748-9326/ac417e.
Rantanen, M., Karpechko, A.Y., Lipponen, A., Nordling, K., Hyvärinen, O., Ruosteenoja, K., Vihma, T., Laaksonen, A., 2022. The Arctic has warmed nearly four times faster than the globe since 1979. Commun. Earth Environ. 3 (1). https://doi.org/10.1038/s43247-022-00498-3.
Reichle, L.M., Epstein, H.E., Bhatt, U.S., Raynolds, M.K., Walker, D.A., 2018. Spatial heterogeneity of the temporal dynamics of Arctic tundra vegetation. Geophys. Res. Lett. 45 (17), 9206–9215. https://doi.org/10.1029/2018GL078820.
Revelle, W., 2025. Procedures for Psychological, Psychometric, and Personality Research. https://CRAN.R-project.org/package=psych.
Romanovsky, V.E., Osterkamp, T., 2000. Effects of Unfrozen Water on Heat and Mass Transport in the Active Layer and Permafrost Article in Permafrost and Periglacial Processes. https://doi.org/10.1002/1099-1530(200007/09)11:33.0.CO;2-7.
Rouse, J.W., Haas, R.H., Scheel, J.A., Deering, D.W., 1974. Monitoring vegetation systems in the great plains with ERTS. In: 3rd Earth Resource Technology Satellite (ERTS) Symposium, pp. 48–62. https://ntrs.nasa.gov/citations/19740022614.
Saccone, P., Hoikka, K., Virtanen, R., 2017. What if plant functional types conceal species-specific responses to environment? Study on arctic shrub communities. Ecology 98 (6), 1600–1612. https://doi.org/10.1002/ecy.1817.
Sakowska, K., Alberti, G., Genesio, L., Peressotti, A., Delle Vedove, G., Gianelle, D., Colombo, R., Rodeghiero, M., Panigada, C., Juszczak, R., Celesti, M., Rossini, M., Haworth, M., Campbell, B.W., Mevy, J.P., Vescovo, L., Cendrero-Mateo, M.P., Rascher, U., Miglietta, F., 2018. Leaf and canopy photosynthesis of a chlorophyll deficient soybean mutant. Plant Cell Environ. 41 (6), 1427–1437. https://doi.org/10.1111/pce.13180.
Salzano, R., Cerrato, R., Scoto, F., Spolaor, A., Valentini, E., Salvadore, M., Esposito, G., Sapio, S., Taramelli, A., Salvatori, R., 2023. Detection of winter heat wave impact on surface runoff in a periglacial environment (Ny-Ålesund, Svalbard). Remote Sens. 15 (18). https://doi.org/10.3390/rs15184435.
Santi, G., Proietti, S., Moscatello, S., Stefanoni, W., Battistelli, A., 2015. Anaerobic digestion of corn silage on a commercial scale: Differential utilization of its chemical constituents and characterization of the solid digestate. Biomass Bioenergy 83, 17–22. https://doi.org/10.1016/j.biombioe.2015.08.018.
Sauter, J.J., Wellenkamp, S., 1998. Seasonal changes in content of starch, protein and sugars in the twig wood of *Salix caprea* L. Holzforschung 52 (3), 255–262. https://doi.org/10.1515/hfsg.1998.52.3.255.
Scartazza, A., Moscatello, S., Gavrichkova, O., Buia, M.C., Lauteri, M., Battistelli, A., Brugnoli, E., 2017. Carbon and nitrogen allocation strategy in Posidonia oceanica is altered by seawater acidification. Sci. Total Environ. 607, 954–964. https://doi.org/10.1016/j.scitotenv.2017.06.084.
Schneider, C., Rasband, W., Eliceiri, K., 2012. NIH Image to ImageJ: 25 years of image analysis. Nat. Methods 9, 671–675. https://doi.org/10.1038/nmeth.2089.
Serreze, M.C., Francis, J.A., 2006. The arctic amplification debate. Clim. Chang. 76 (3–4), 241–264. https://doi.org/10.1007/s10584-005-9017-y.
Sjögersten, S., Van Der Wal, R., Woodin, S.J., 2006. Small-scale hydrological variation determines landscape CO2 fluxes in the high Arctic. Biogeochemistry 80 (3), 205–216. https://doi.org/10.1007/s10533-006-9018-6.
Sulman, B.N., Salmon, V.G., Iversen, C.M., Breen, A.L., Yuan, F., Thornton, P.E., 2021. Integrating Arctic plant functional types in a land surface model using above- and belowground field observations. J. Adv. Model. Earth Syst. 13 (4). https://doi.org/10.1029/2020MS002396.
Tarnocai, C., Canadell, J.G., Schuur, E.A.G., Kuhry, P., Mazhitova, G., Zimov, S., 2009. Soil organic carbon pools in the northern circumpolar permafrost region. Glob. Biogeochem. Cycles 23, GB2023. https://doi.org/10.1029/2008GB003327.
Tejnecký, V., Luláková, P., Šantrůčková, H., Křížová, P., Lehejček, J., Hájek, T., Mercl, F., Bárta, J., Němeček, K., Drábek, O., 2025. Arctic willow (Salix polaris) exudation as a

driver of microbial activity and soil formation in the high arctic tundra. Biogeochemistry 168 (2). https://doi.org/10.1007/s10533-025-01222-x.
Van Der Wal, R., Bardgett, R.D., Harrison, K.A., Stien, A., 2004. Vertebrate herbivores and ecosystem control: cascading effects of faeces on tundra ecosystems. Ecography 27 (2), 242–252. https://doi.org/10.1111/j.0906-7590.2004.03688.x.
Van der Wal, R., Stien, A., 2014. High-arctic plants like it hot: a long-term investigation of between-year variability in plant biomass. Ecology 95 (12), 3414–3427. https://doi.org/10.1890/14-0533.1.
von Oppen, J., Assmann, J.J., Bjorkman, A.D., Treier, U.A., Elberling, B., Nabe-Nielsen, J., Normand, S., 2022. Cross-scale regulation of seasonal microclimate by vegetation and snow in the Arctic tundra. Glob. Chang. Biol. 28 (24), 7296–7312. https://doi.org/10.1111/gcb.16426.
Wang, J., Wen, X., 2022. Limiting resource and leaf functional traits jointly determine distribution patterns of leaf intrinsic water use eeciency along aridity gradients. Front. Plant Sci. 13. https://doi.org/10.3389/fpls.2022.909603.
Welker, J.M., Molau, U., Parsons, A.N., Robinson, C.H., Wookey, P.A., 1997. Responses of Dryas octopetala to ITEX environmental manipulations: a synthesis with circumpolar comparisons. Glob. Chang. Biol. 3 (1), 61–73. https://doi.org/10.1111/j.1365-2486.1997.gcb143.x.
Welker, J.M., Wookey, P.A., Parsons, A.N., Press, M.C., Callaghan, T.V., Lee, J.A., 1993. Leaf carbon isotope discrimination and vegetative responses of Dryas octopetala to temperature and water manipulations in a High Arctic polar semi-desert, Svalbard. Oecologia 95, 463–469. https://doi.org/10.1007/BF00317428.
Wenzl, M., Baumhoer, C.A., Dietz, A.J., Kuenzer, C., 2024. Vegetation changes in the arctic: a review of earth observation applications. In: Remote Sensing, Vol. 16. Multidisciplinary Digital Publishing Institute (MDPI). https://doi.org/10.3390/rs16234509. Number 23.
Wickham, H., 2016. ggplot2: Elegant Graphics for Data Analysis. Springer-Verlag, pp. 189–201. https://doi.org/10.1007/978-3-319-24277-4_9.
Wickham, H., Averick, M., Bryan, J., Chang, W., McGowan, L., François, R., Grolemund, G., Hayes, A., Henry, L., Hester, J., Kuhn, M., Pedersen, T., Miller, E., Bache, S., Müller, K., Ooms, J., Robinson, D., Seidel, D., Spinu, V., Yutani, H., 2019. Welcome to the Tidyverse. J. Open Source Softw. 4 (43), 1686. https://doi.org/10.21105/joss.01686.
Wilkman, E., Zona, D., Tang, Y., Gioli, B., Lipson, D.A., Oechel, W., 2018. Temperature response of respiration across the heterogeneous landscape of the Alaskan Arctic Tundra. J. Geophys. Res. Biogeosci. 123 (7), 2287–2302. https://doi.org/10.1029/2017JG004227.
Xue, K., Yuan, M., Shi, J., Qin, Y., Deng, Y., Cheng, L., Wu, L., He, Z., Van Nostrand, J.D., Bracho, R., Natali, S., Schuur Edward, A.G., Luo, C., Konstantinidis, K.T., Wang, Q., Cole, J.R., Tiedje, J.M., Luo, Y., Zhou, J., 2016. Tundra soil carbon is vulnerable to rapid microbial decomposition under climate warming. Nat. Clim. Chang. 6 (6), 595–600. https://doi.org/10.1038/nclimate2940.
Yazbeck, T., Bohrer, G., Sonnentag, O., Qu, B., Detto, M., Hould-Gosselin, G., Graveline, V., Alcock, H., Lecavalier, B., Marsh, P., Cannon, A., Riley, W.J., Zhu, Q., Yuan, F., Sulman, B., 2025. Shrub Expansion Can Counteract Carbon Losses From Warming Tundra. J. Geophys. Res. Biogeosci. 130 (8). https://doi.org/10.1029/2024JG008721.
Zagajewski, B., Kycko, M., Tømmervik, H., Bochenek, Z., Wojtuń, B., Bjerke, J.W., Kłos, A., 2018. Feasibility of hyperspectral vegetation indices for the detection of chlorophyll concentration in three high Arctic plants: Salix polaris, Bistorta vivipara, and Dryas octopetala. Acta Soc. Bot. Pol. 87 (4). https://doi.org/10.5586/asbp.3604.
Zarco-Tejada, P., Berjón, A., López-Lozano, R., Miller, J., Martín, P., Cachorro, V., González, M., de Frutos, A., 2005. Assessing vineyard condition with hyperspectral indices: leaf and canopy reflectance simulation in a row-structured discontinuous canopy. Remote Sens. Environ. 99 (3), 271–287. https://doi.org/10.1016/j.rse.2005.09.002.
Zhou, Y., Yang, M., Tai, Z., Jia, J., Luan, D., Ma, X., 2022. Carbohydrates and secondary compounds of alpine tundra shrubs in relation to experimental warming. BMC Plant Biol. 22 (1), 482. https://doi.org/10.1186/s12870-022-03851-y.
Zibulski, R., Wesener, F., Wilkes, H., Plessen, B., Pestryakova, L.A., Herzschuh, U., 2017. C/N ratio, stable isotope (δ13C, δ15N), and n-alkane patterns of brown mosses along hydrological gradients of low-centred polygons of the Siberian Arctic. Biogeosciences 14 (6), 1617–1630. https://doi.org/10.5194/bg-14-1617-2017.
Zona, D., Lafleur, P.M., Hufkens, K., Gioli, B., Bailey, B., Burba, G., Euskirchen, E.S., Watts, J.D., Arndt, K.A., Farina, M., Kimball, J.S., Heimann, M., Göckede, M., Pallandt, M., Christensen, T.R., Mastepanov, M., López-Blanco, E., Dolman, A.J., Commane, R., Oechel, W.C., 2023. Pan-Arctic soil moisture control on tundra carbon sequestration and plant productivity. Glob. Chang. Biol. 29 (5), 1267–1281. https://doi.org/10.1111/gcb.16487.
Zuur, A.F., Ieno, E.N., Elphick, C.S., 2010. A protocol for data exploration to avoid common statistical problems. Methods Ecol. Evol. 1 (1), 3–14. https://doi.org/10.1111/j.2041-210X.2009.00001.x.